Electrical properties of cement-based materials: Multiscale modeling and quantification of the variability

Tulio Honorio, Helena Carasek, Oswaldo Cascudo

Electrical properties of cement-based materials: multiscale modeling and quantification of the variability

Tulio Honorio[a,*], Helena Carasek[b], Oswaldo Cascudo[b]

[a] *Université Paris-Saclay, ENS Paris-Saclay, CNRS, LMT - Laboratoire de Mécanique et Technologie, 94235, Cachan, France*
[b] *Universidade Federal de Goiás, Escola de Engenharia Civil e Ambiental, PPG-GECON, Goiânia, Brazil*

Abstract

The electrical properties, resistivity and conductivity, inform on the durability of cement-based materials and can be used for monitoring and inspection of concrete structures. The physical origin of these properties can be linked to the dynamics of the pore solution. We propose a multiscale modeling approach of the electrical conductivity and resistivity informed by the dynamics of ions that enables the quantification of property variability across scales using Monte Carlo Micromechanics (MCM) computations. As a source of variability, we consider the pore solution composition, clinker composition and the uncertainty on solid conductivity. The results are compared to experimental measurements on various cement systems. The age-dependency of ionic diffusion, due to ion-ion and ion-solvent collective effects, is crucial to model the evolution of electrical conductivity. The main results show that Monte Carlo Micromechanics enables the quantification of the variability and uncertainty across scales, since MCM computations have provided estimates of the standard deviation of the electrical conductivity and resistivity at the scales of cement paste, mortar and concrete. Also, the results show that self-consistent scheme provides a good estimate of the effective electrical conductivity of cement-pastes, capturing the transition from a liquid to a solid matrix during cement hydration.

*Corresponding author
Email address: tulio.honorio-de-faria@ens-paris-saclay.fr (Tulio Honorio)

Keywords: Electrical resistivity; Electrical conductivity; Specific ion effects; Composition variability; Micromechanics.

Highlights

- Self-Consistent scheme captures the age-evolution of the electrical conductivity
- Micromechanics Monte Carlo enables variability quantification across scales
- The effects of pore solution variability on the resistivity up to the concrete scale are quantified.

1. Introduction

Measurements of electrical conductivity ($\sigma = 1/\rho$, which is the reciprocal of the electrical resistivity ρ) have been widely used for monitoring and inspection of concrete structures, especially in the assessment of corrosion severity, carbonation evolution, quality control of concrete structures and cement hydration development [1, 2, 3], setting time and shrinkage [3, 4]. The electrical conductivity informs on the inter-connectivity of pores in cement-based materials, directly correlating with ionic diffusion and water permeability [5, 6]. The formation factor F, defined as the ratio between the effective conductivity of the material $\sigma(t)$ and the conductivity of the pore phase (e.g. [7]), has been used as a key indicator of ion transport through cement-based materials [6, 8] and other porous media [7]. The permeability of a porous media scales as $1/F$: $k \propto l_c^2/F$, where l_c is a length scale associated with the pores. A rigorous link between diffusion coefficients D, relaxation time T_1 (that can be obtained from NMR experiments), permeability k and the formation factor is given by [7]: $k \leq DT_1/F$. Cross-property relations between electrical conductivity and elastic properties have also been identified [9, 10]. These aspects show that measurements of electrical properties enable to assess important information related to durability processes and the evolution of the porosity in cement-based materials.

The electrical resistivity of concrete is known to vary over a wide range: 10 to 10^6 Ω.m [2, 11]. Such variability is due to the dependence of the electrical resistivity on the [2, 6]:

- **Pore solution composition**, which depends on the composition of the binder (Portland cement and Supplementary Cementitious Materials (SCM)), age, temperature, and service environment (e.g. marine exposure, chemical alterations) [12, 13]. Molecular modeling shows that the composition and dynamics of ions are directly related to the electrical conductivity of the pore solutions [14].

- **Moisture content or relative humidity (RH)**. The electrical conductivity increases with the content of evaporable water in cement-based materials [6]. Although the diminution of the (internal) RH is accompanied by an increase in the concentration of ions in the liquid phase within the pores, only smaller pores remain saturated under RH decrease and the inter-connectivity of pores with (liquid) aqueous solutions is jeopardized.

- **Temperature**. The electrical conductivity is reported to increase with the temperature. According to Polder et al. [2], the temperature dependence of the electrical conductivity of the bulk pore solution differs from the ones of cement paste and mortar. The resistivity is reported [2] to increase approximately r_T= 3 to 5 % per degree Celsius (i.e. $\rho \propto r_T T$), which means that the conductivity scales with $\sigma \propto \frac{s_T}{T}$ with $s_T = 20$ to 33. The thermo-activation of the conductivity ($\frac{s_T}{T}$) can be modeled using an Arrhenius factor [8].

- **Pore structure**. Christensen et al. [6] note that the electrical conductivity of cement-based materials is directly related to the pore volume fraction and inter-connectivity, being a good estimation of the latter in evolving cement systems. This means that a potentially relevant, but still to be quantified, contribution of the morphological aspects of the pore system may exists in estimation of the conductivity or resistivity of cement-based

materials.

Micromechanics techniques have been extensively used to establish composition/(micro)structure/property correlations for heterogeneous materials. Multiscale studies of the electrical properties of cement-based materials have been proposed using analytical [6, 15] and numerical [15, 16, 4] homogenization tools. Numerical homogenization based on microstructural simulation [17, 18, 19, 16] has also successfully applied to get insights on the structuration and to study the various properties of interest of cement-based materials. However, it is a challenge to simulate an actual Representative Elementary Volume (REV), accounting for the real size distribution of the heterogeneities in cement-based materials. To illustrate, let us consider a typical cement particle size distribution ranging from 0.1 to 100 μm (e.g. [20]). To analyze a representative numerical sample of a cement paste using, for example, finite elements method, it would be necessary a REV on the order of a millimeter (ten-fold the size of the larger heterogeneity) while the minimum element size would be on the order of 0.1 μm. In a 3D simulation, the total number of degrees of freedom (DOF) on the order of 10^{12} is prohibitive. A fallback solution often employed is to limit the range of heterogeneity size considered so that DOF does not exceed a few 10^7. But in this case, it would be advisable to analyze several numerical samples to get a relevant statistical description of the disordered material. Such numerical homogenization approaches seem, therefore, not very well suited to investigations aiming at quantifying the variability of complex heterogeneous materials, which requires a large number of evaluations per scenario. The simplicity of micromechanics-based computations enables to test several scenarios of interest regarding the composition, uncertainty on phase properties and morphology of phases (e.g. in terms of matrix/inclusions or polycrystalline morphologies, and inclusion shape) of a composite.

A complete characterization of the microstructure of cement-based materials is a huge challenge. Even if one bases the analysis on microstructures experimentally probed (for instance using tomography) on a given cement system and

mix design, there is no guarantee that the same microstructure is representative of other cement systems. In this context, the strategy that is often adopted in the framework of micromechanics is to start the analysis from the most basic features that are shared by all cement systems: a multiscale microstructure that can be approximated as a random heterogeneous material. The theory provides tools enabling to take into account, often in an approximate way, the effects of shape, inclusion orientation and distribution [21], allowing the quantification of the relative contribution of these microstructural features.

The randomness of physical properties and volume fraction of the different constituents of composites (at the microscopic scale) are recognized as a critical factor leading to variability in the effective properties at the macroscopic scale [22, 23]. The effects of various sources of variability presented on the effective resistivity of cement-based materials have been studied by Lataste et al. [24]. These authors also point out the variability related to concrete casting and on-site *versus* laboratory measurements. A multiscale modeling approach accounting for the variabilities at the material level is still to be proposed to cement-based materials.

In this work, we propose a multiscale modeling approach informed by the dynamics of ions (at the molecular scale). Furthermore, we introduce an analytical homogenization approach in which probability distributions are used to capture the variabilities related to the composition and property uncertainty on the electrical properties of cement-based materials. The probability distributions associated with the variability of the electrical conductivity of the pore solutions are used as input in micromechanics in order to upscale the electrical conductivity and resistivity, and the respective the variability, across scales. For validation, modeling results are compared to experimental measurements on various cement systems. Our results represent an advance in the multiscale modeling of cement-based materials informed by the nanoscale and in reducing the empirism of investigations based on the resistivity of concrete.

The article is organized as follows. First, the micromechanics schemes used to model the conductivities are presented and we introduce the Monte Carlo

Micromechanics (MCM) technique to estimate the variability in effective properties in a multiscale framework. Then, we apply micromechanics theory to upscale cement paste, ITZ, mortar and concrete conductivity and resistivity, as well as the associated variability computed with MCM.

2. Micromechanics of the electrical properties

Micromechanics is the study of the mechanical, thermal, electromagnetic and mass transport behavior of the materials with a microstructure [25]. The results of micromechanics can be used to upscale (i.e. to obtain the effective properties of heterogeneous materials) or downscale (i.e. to obtain the specific properties of a given constituent by inverse analysis).

2.1. Homogenization of the electrical conductivity

The homogenization of the electrical conductivity is analogous to the homogenization of the thermal conductivity, dielectric permittivity, and diffusion coefficient [9]. In this section, we recall three homogenization schemes - namely Mori-Tanaka (MT), Self-Consistent (SC) and the Generalized Self-Consistent (GSC) schemes - that have been extensively used (e.g.[26, 27, 28, 29, 30, 31, 32, 33]) to estimate the effective properties of cement-based materials accounting for the hierarchical microstructure of the material. With these homogenization schemes, it is possible to account for the random nature of cement-based materials microstructure and interactions among the different phases (in a simplified way). As will be presented in more detail, even complex phenomena related, for example, to the setting of cement and microstructure development can be fairly well captured by the combination of these schemes, which make them an ideal tool to model early-age property development. With analytical homogenization schemes, the estimations are computer inexpensive compared to numerical homogenization based on finite element methods. In investigations coping with the variability of the materials, in which a large number of evaluations are needed, analytical homogenization arises as an ideal candidate to evaluate effective properties.

In a matrix/inclusion morphology, for a (N+1)-phase heterogeneous material with N isotropic spherical inclusions randomly distributed in a representative elementary volume, the Mori-Tanaka (or Maxwell-Garnett) estimation of the effective electrical conductivity σ^{MT} can be computed from [9]:

$$\frac{\sigma^{MT} - \sigma_0}{\sigma^{MT} + 2\sigma_0} = \sum_{r=1}^{N} f_r \frac{\sigma_r - \sigma_0}{\sigma_r + 2\sigma_0} \tag{1}$$

where f_r is the volume fraction of the phase r, and the subscript $_0$ denotes the (isotropic) matrix phase.

For a two-phase material, Mori-Tanaka estimation corresponds to the Hashin-Shtrikman (HS) bounds, which are the tightest bounds that can be defined for a two-phase composite. HS upper and lower bounds are obtained by interchanging the subscripts in MT estimates. Assuming $\sigma_0 > \sigma_1$ the upper and the lower HS bounds are, respectively [34]:

$$\sigma_+^{HS} = \sigma_0 + \frac{f_1}{\frac{1}{\sigma_1 - \sigma_0} + \frac{f_0}{3\sigma_0}} \tag{2}$$

$$\sigma_-^{HS} = \sigma_1 + \frac{f_0}{\frac{1}{\sigma_0 - \sigma_1} + \frac{f_1}{3\sigma_1}} \tag{3}$$

Note that these results were derived for the effective magnetic permeability, but as originally stated by Hashin and Shtrikman [34], they also hold for the electric conductivity, thermal conductivity, and diffusivity of composite materials due to due to mathematical analogy.

In a polycrystalline-like morphology, for a N-phase heterogeneous materials with N isotropic equiaxed inclusions randomly distributed in representative elementary volume, the Self-Consistent (or Bruggeman) estimation of the effective electrical conductivity σ^{SC} can be computed from the implicit formula [9]:

$$\sum_{r=1}^{N} f_r \frac{\sigma_r - \sigma^{SC}}{\sigma_r + 2\sigma^{SC}} = 0 \tag{4}$$

where f_r is the volume fraction of the phase r.

Using the consistency condition $\sum_r^N f_r = 1$, for a two-phase material, the SC estimation is explicit and given by:

$$\sigma_2^{SC} = \frac{1}{4}\left(S_{SC} + \sqrt{S_{SC}^2 + 8\sigma_1\sigma_2}\right) \tag{5}$$

with $S_{SC} = ((3f_1 - 1)\sigma_1 + (2 - 3f_1)\sigma_2)$.

The presence of interphases (i.e. the volume in-between two phases - in contrast with an "interface", which is a surface between two surfaces) can be modeled with the Generalized Self-Consistent (GSC) scheme based on the composite-sphere morphology. GSC scheme has been widely deployed to model the mechanical and transport properties of the ITZ [26, 35, 36, 37, 38]. The GSC results for effective conductivities (thermal, electrical, diffusivities etc) is the recursive equation (e.g. [39, 9]):

$$\overline{\sigma_i^{GSC}} = \sigma_i + \frac{1 - f_i}{\frac{1}{\sigma_{i-1} - \sigma_i} + \frac{f_i}{3\sigma_i}} \tag{6}$$

where $\overline{\sigma_i^{GSC}}$ is the effective conductivity of a matrix/composite-sphere composite in which the composite-sphere is constituted of $(i-1)$ concentric coats and a core (associated here to subscript 0) embedded in a matrix (here, represented by the subscript i). With simple manipulations, it is possible to show that this form for a 2-phase material is equivalent to that of a 2-phase MT scheme.

2.2. Quantification of the variability and uncertainty using Monte Carlo Micromechanics (MCM)

In order to quantify the effects of variability and uncertainty of phase constituents at the macroscale response of the heterogeneous materials, we deploy a strategy that we name Monte Carlo Micromechanics (MCM) hereafter. MCM consists at computing the effective properties (in Eqs. 1 and 4, for instance) assuming that the input (i.e. effective properties and volume fractions) are described by a *probability density function* (PDF). Similar approaches have been proposed in the literature to quantify the variability and uncertainty of other physical properties of composites [22] and biomaterials [40]. Note that, due to

the consistency condition $\sum_{r=1}^{N} f_r = 1$, therefore only $(N-1)$ volume fractions are independent variables. The PDF of the effective properties can be then computed by sampling the parameters of interest according to their respective PDF and then evaluating the micromechanics estimations of the effective properties. The procedure is to be performed N_{MC} times, with the convergence (which scales as $1/\sqrt{N_{MC}}$) ensured by the sound statistical foundations of MC methods.

For a given continuous PDF $f(X)$, the mean is given by $\mu_X = \mathbb{E}[X] = \int x f(x) dx$, and the variance by $s_X^2 = \mathbb{E}[(f(x) - \mu_X)^2] = \int x^2 f(x) dx - (\mu_X)^2$. In the following, we adopt the Log-Normal distribution (i.e. a distribution in which the logarithm of a random variable is normally distributed):

$$f(x; \mu_G, s_G) = \frac{1}{x s_X \sqrt{2\pi}} \exp\left[-\frac{(\ln x - \mu_X)^2}{2 s_X^2} \right] \tag{7}$$

where μ_G and s_G are, respectively, the mean and standard deviation of the random variable logarithm, to describe the PDF of the properties and volume fractions. The Log-Normal distribution is an adequate choice of the PDF here because it avoids negative (nonphysical) properties and volume fractions. To avoid volume fractions exceeding 1, the volume fractions obtained in a given trial can simply by renormalized. The mean and the standard deviation of the Log-Normal distribution are given, respectively, by $\mu_{LN} = \exp\left(\mu_G + \frac{s_G^2}{2}\right)$ and $s_{LN} = \sqrt{\left(e^{(s_G^2)} - 1\right) e^{(2\mu_G + s_G^2)}}$.

In Appendix A, we discuss the convergence of MCM estimations and compare them to analytical results obtained in the simplest case of a mixture rule.

2.3. Simplified modelling of the conductivity of the pore solution and variability

We show in a recent study that the age-dependency of the electrical conductivity of the pore solution, for various cement systems, can be approximated by the following empirical relation [41]:

$$\sigma_{PS}(w/c) = \frac{1}{w/c} \left(4.560 - 2.881 e^{-t/0.975} \right) \tag{8}$$

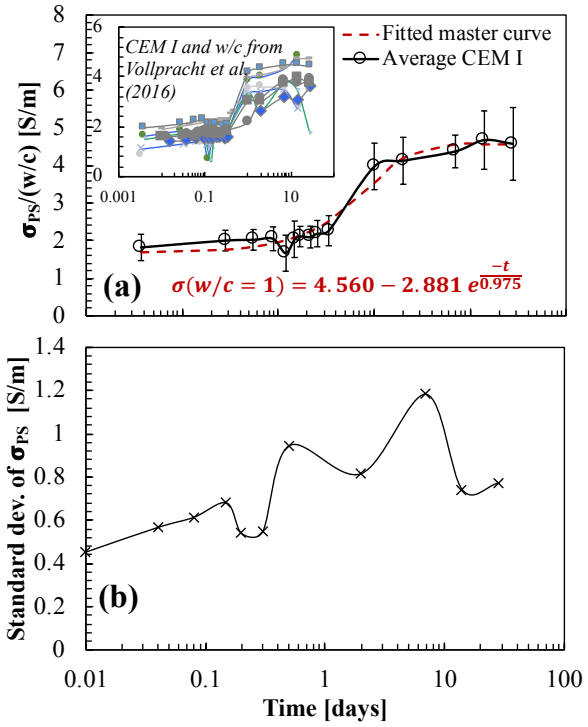

Figure 1: (a) Master curve obtained from averaging experimental conductivity provided in Vollpracht et al. [13] database (value shown in the inset). (b) Standard deviation, computed from the experimental data, as a function of the time.

for σ in S/m and t in days. This expression is consistent with experimental data [13] and theoretical considerations based on the molecular hydrodynamics of the pore solutions[41, 14, 42]. This expression is plotted in Fig. 1 (a) and compared to the averages of the normalized experimental data from Vollpracht et al. [13] (shown in the inset). The standard deviation, computed from the experimental data, is plotted as a function of the time in Fig. 1 (b).

3. Results

3.1. Cement, hydrates, pores and aggregates: evolution of volume fractions and effective conductivity per phase

To obtain the evolution of the volume fractions of hydrates, we employ two simplified models: Powers [43] and Tennis and Jennings [44] models. The details of each model are presented in Appendix B. With Powers model, the volume fractions of clinker, hydrates, and capillary porosity, as well as chemical shrinkage, are provided as a function of the degree of hydration, w/c ratio and mass volume of water and cement. The hydrates are treated as a homogeneous phase. Even if the pore solution is the main contributor to the electrical response of cement-based materials, a precise quantification of the electrical properties of the hydrates can enhance the accuracy of the interpretation of resistivity results (being the reciprocal of the conductivity, the lower values of conductivity impact more the resistivity). Recently, it was shown that accounting for the partition of hydrates in cement paste could lead to significant differences in the estimates of effective elastic properties of cement paste [45]. In this context, Tennis and Jennings [44] model is convenient since it enables the computation (based on simplified assumption regarding phase assemblage in CEM I systems) of the evolution of each clinker mineral and gypsum fractions as well as the main hydrates including high- and low-density C-S-H, CH, and the Al-bearing phases: ettringite ($C_6A\bar{S}_3H_{32}$ or AFt), monosulfoaluminate ($C_4A\bar{S}H_{12}$ or AFm), hydrogarnet ($C_3(A,F)H_6$) and C_4AH_{13}, all in cement notation. The volume fraction of the gel pores in C-S-H is also provided.

Figure 2 shows a comparison between the estimations of that can be obtained with Powers, and Tennis and Jennings models. Further, we provide MCM computations using as input the variability in clinker and gypsum fractions encountered in typical CEM I. The probability distribution functions of the mass fraction of clinker and gypsum in CEM I composition as proposed in ref. [45] based on Taylor [46] is shown in Fig. 2 (a). Using Tennis and Jennings model, we show in Fig. 2 (b) the mean volume fractions of various phases in a

cement system as a function of the w/c ratio for a degree of hydration of α of 0.8. A normal distribution was adopted but it can be shown that using a uniform distribution lead only to slighter larger standard deviations in the volume fractions [45] (a simple visual analysis of Fig. 2 (a) shows that with the variability adopted for clinker mineral fractions remain in the domain of positive fractions) . The comparison between the Powers and Tennis and Jennings estimates of hydrates, capillary porosity, and chemical shrinkage is presented in Fig. 2 (c) for a degree of hydration of α of 0.8, which is a typical value associated with late ages in cement-based materials. The volume fraction of hydrates obtained from Powers model is slightly larger than the ones obtained with Tennis and Jennings model. The inverse is observed in capillary porosity estimates. In both cases, the differences observed are not within the variability associated with CEM I composition variability depicted by the error bars. Thus, if one assumes that the electrolytes within the gel porosity also contribute to the electrical conduction, the total "conductive" porosity is still larger when one adopts Tennis and Jennings model.

A possible issue with using a more detailed description of phases assemblage in cement pastes is that the precise values of the properties of each phase may not be known. On the other hand, non-porous solid phases are expected to exhibit very low electrical conductivity (i.e. they can be treated *effectively* as insulators). Clinker minerals, CH, and hydrogarnet do not present micropores (i.e. pores <2 nm according to the IUPAC) in their atomic structure whereas C-S-H exhibits interlayer micropores and gel mesopores (i.e. pores ranging from 2 to 50 nm according to the IUPAC). The space in between the columns in ettringite and the interlayer pores in AFm phases can be viewed as micropores; the dynamics of water and sulfates are expected to the be slowed down by the high confinement as captured in molecular dynamics simulations [47] (similar reasoning would apply to the other counter-anions as hydroxide and chloride that can appear in AFm phases). In this context, C-S-H would be expected to exhibit a non-zero electrical conductivity due, at least, to the mesopores whilst the other hydrates could be treated as insulators.

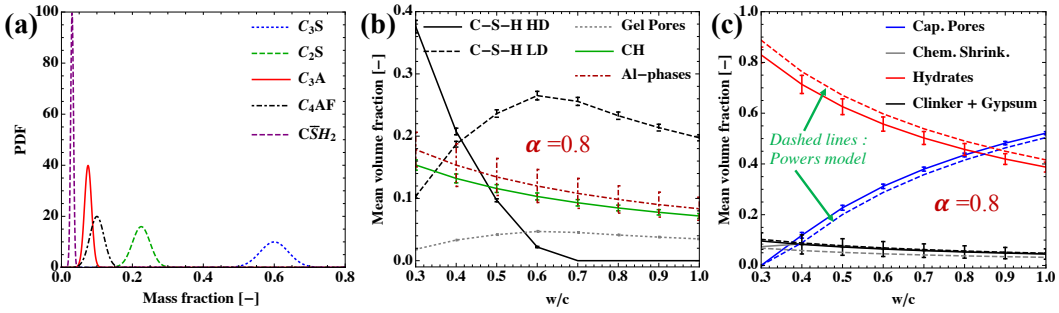

Figure 2: (a) Probability distribution functions of the mass fraction of clinker and gypsum in CEM I composition as proposed in ref. [45] based on Taylor [46]. (b) Mean volume fraction of various phases in a cement system as a function of the w/c ratio obtained using Tennis and Jennings model for a degree of hydration of α of 0.8 (a typical value associated with late ages in cement-based materials). The volume fractions of all aluminum bearing phases (AFt, AFm, hydrogarnet and C_4AH_{13}) are grouped. MCM computations using the PDF in (a) were performed with $N_{MC} = 10000$ to get the mean values, the error bars correspond to the standard deviations. (c) Volumes fractions of hydrates, cement, capillary pores and chemical shrinkage as obtained from Tennis and Jennings and from Powers models. The error bars correspond to the standard deviations from MCM computations.

With these arguments, we propose the representation of the multiscale hierarchical microstructure of cement-based materials, from C-S-H up to concrete scale, presented in Fig. 3. The length scales associated with each level give support to the separation of scales proposed (similar scale separation has also been adopted in other studies dealing with the homogenization of various physical properties of cement-based materials [32, 48]). Four levels are considered :

- *Level 0 - C-S-H LD*: The effective properties of C-S-H LD are computed assuming that the electrolyte in gel pores exhibits an electrical conductivity similar to that of capillary porosity. The effective electrical conductivity of the C-S-H particle σ_{C-S-H} being a parameter to be defined. We adopt the polycrystal-like morphology corresponding to SC estimate to upscale the electrical conductivity at this level. No specific steps are introduced to take into account the densification processes of C-S-H. Experimental [49] and theoretical [50, 51] evidences suggests a mechanism of densification of C-S-H as hydration processes develop. Since the electrical conductivity of the C-S-H in its high and low density forms are at least one order of magnitude lower (following the discussion in the next section) than the conductivity of the pore solution, the effects of densification are not expected to be significant on the upscaling of the effective conductivity of cement-based materials across scale. A discussion in the Appendix B.2 shows however that in some conditions Tennis and Jennings [44] model implies a densification of C-S-H.

- *Level 1 - Cement Paste*: The effective properties of the cement paste are computed considering the capillary pores and C-S-H (HD with a conductivity σ_{C-S-H} and LD with a conductivity obtained from homogenization in level 0) as conductor phases and other hydrates, gypsum, and clinker as insulator phases. Both matrix/inclusion and polycrystal-like morphologies are tested in the following.

- *Level 2 - Mortar*: The effective properties of the mortar are obtained considering a matrix/inclusion morphology with the fine aggregate particles

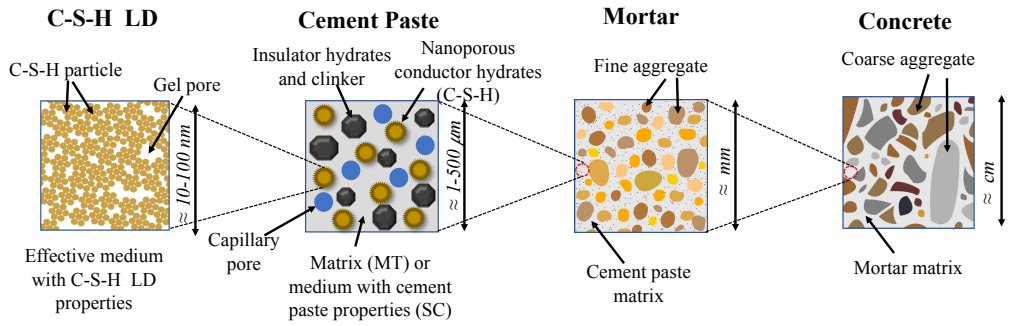

Figure 3: Representation of the multiscale hierarchical microstructure of cement-based materials. In the application of the homogenization schemes, we approximate the shape of all heterogeneities depicted by spherical inclusions (or equiaxed inclusions in the case of SC scheme).

embedded in a cement paste matrix. We assume non-porous aggregates, which behave effectively as insulators. For the sake of simplicity, we do not consider the ITZ. See Appendix C for a throughout the discussion on the role of ITZ in the electrical conductivity. In the absence of information on the particle size distribution of aggregates and on the ITZ characterization, neglecting the ITZ seems a reasonable assumption.

- *Level 3 - Concrete*: The effective properties of the concrete are obtained considering a matrix/inclusion morphology with the coarse aggregates embedded in a mortar matrix. Again, no ITZ is considered and non-porous insulator aggregates are assumed.

3.2. Effective electrical properties: from C-S-H particles up to cement paste

A first estimate of the effective electrical conductivity of the C-S-H particle σ_{C-S-H} can be obtained from the diffusion coefficients. If one assumes that only the pore solution contributes to the overall conductivity (i.e. the conductivities of the other phases are 0), then Eq. 5 shows that the ratio between the effective conductivity and the conductivity of the pore solution $\sigma^{eff}/\sigma_{PS} = \frac{1}{2}(3\phi - 1)$ is

a constant that depends only on the capillary porosity of the system. Nernst-Einstein relation links the self-diffusion coefficient D_i of a given ion species i to the conductivity of the ion σ_i in the electrolytes in approximate manner [52]: $\sigma_i = \frac{z_i^2 c_i F^2 D_i}{RT}$, where c_i is the ionic concentration, $\mathcal{F}$ and R_g are the Faraday and gas constants, respectively. This relation is known to overestimate the conductivity of ionic solutions [53] but is a reasonable approximation for pore solution in cement-based as discussed in details by us in ref. [41]. Indeed, this relation has been successfully used to model pore solution in cement-based materials [54, 15, 55]. Assuming Nernst-Einstein relation, in a system with homogeneous dynamics (i.e. $D_i = D_h$ for all ion i, as in the Case A in the previous Part), one obtains $\sigma^{eff}/\sigma_{PS} = D_{eff}/D_{PS}$, where D_{eff} is the effective diffusion coefficient of the porous medium (which can also be obtained from SC or MT schemes presented in section 2.1 but using the diffusion of each phase as input instead of the conductivities) and $D_{PS} = D_h$ is the diffusion coefficient associated to the ionic species of the pore solution. In an attempt to estimate the electrical conductivity of C-S-H from diffusion coefficients, various authors obtained values of $\sigma_{C-S-H}/\sigma_{PS}$ ranging from 0.0025 to 0.01 [56, 15, 57, 58]. It must be noted, however, that the underlying assumption of homogeneous dynamics can be problematic in multi-component ionic solutions, as discussed in details in ref. [41], and is not sufficient to capture the age-dependency of the conductivity of the pore solutions in cement-based materials. Furthermore, adopting a constant $\sigma_{C-S-H}/\sigma_{PS}(t)$ means that the electrical conductivity of C-S-H σ_{C-S-H} is assumed to be time-dependent.

We assess the sensibility of the effective electrical conductivity of the cement paste with respect to C-S-H electrical conductivity σ_{C-S-H} in Fig. 4 as a function of the w/c, using Tennis and Jennings model to obtain the volume fractions of phases and a first homogenization to upscale C-S-H LD conductivity (SC estimate of a foam composed of solid particles and gel pores - Level 0 as discussed in last section). We use as input in MCM computations the composition variability of clinker in Fig. 2(a) and N_{MC}=10^4. Both SC and MT approaches to upscale cement paste are considered. For the latter, we consider the cases in which

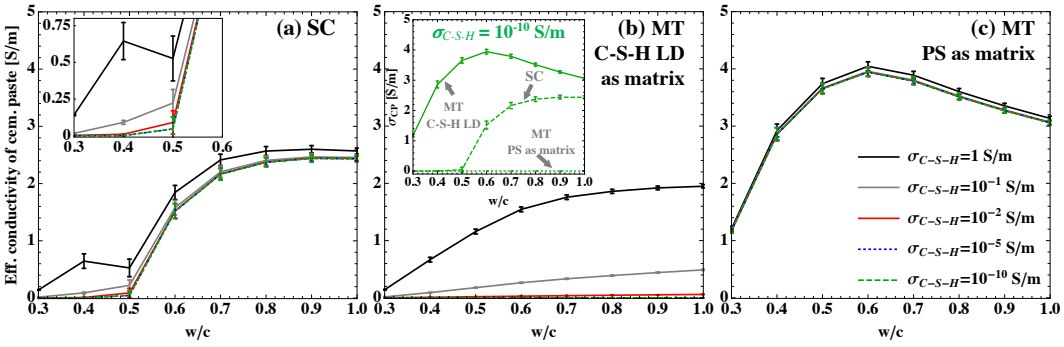

Figure 4: Sensibility of the effective electrical conductivity of the cement paste to C-S-H electrical conductivity: comparison between (a) SC, (b) MT with the C-S-H LD as matrix, and (c) MT with the pore solution as matrix. We used the composition variability of clinker in Fig. 2(a) as input in MCM computations with N_{MC}=10^4. The inset in (a) zooms in the range of w/c ratios typically observed in concretes. The legend in (c) applies to the three figures. The inset in (b) gather the estimates using σ_{C-S-H} =10^{-10} S/m as input.

either C-S-H LD or the pore solution function are the hosting matrix (previous studies on micromechanics of the cement paste also adopted C-S-H LD as the matrix at cement paste level [48, 32, 59]). We used the composition variability of clinker in Fig. 2(a) as input in MCM computations with N_{MC}=10^4. The corresponding standard deviation of the effective electrical conductivity is also shown. The inset in (a) zooms in the MT estimates having the C-S-H LD as the matrix. With SC scheme and MT having the pore solution as matrix, the effective conductivity $\sigma_{CP}(w/c)$ of the cement paste at a given w/c converges to a finite value as $\sigma_{C-S-H} \to 0$ (the curves corresponding to $\sigma_{C-S-H} = 10^{-5}$ and 10^{-10} S/m are indistinguishable). With MT having the C-S-H LD as matrix, $\sigma_{CP}(w/c)$ tends to 0 as $\sigma_{C-S-H} \to 0$. The MT estimates function as bounds to the SC estimates as can be seen in the inset in Fig. 4 (b).

To get the effective conductivity of the solids σ_s accounting for the interactions among the various phases in the system, we use Eqs. 1 and 4 to rewrite the effective properties of the multi-component system as a 2-phase system (solid phase, denoted by the subscript $_s$ and a pore phase denoted by the subscript $_{PS}$). With SC estimate, σ_s can be obtained by solving the following equation

as a function of the effective SC estimate of the electrical conductivity of the cement paste σ_{CP}^{SC}:

$$f_s \frac{\sigma_s - \sigma_{CP}^{SC}}{\sigma_s + 2\sigma_{CP}^{SC}} = f_{LD} \frac{\sigma_{LD} - \sigma_{CP}^{SC}}{\sigma_{LD} + 2\sigma_{CP}^{SC}} - f_{HD} \frac{\sigma_{C-S-H} - \sigma_{CP}^{SC}}{\sigma_{C-S-H} + 2\sigma_{CP}^{SC}} - \frac{f_{NC}}{2} \tag{9}$$

where $f_s = f_{LD} + f_{HD} + f_{NC}$ is total volume fraction of solids, σ_{LD} is the electrical conductivity of C-S-H LD obtained by homogenization, $f_{LD} = f_{LD}^{Sol} + f_{Gel}$ is the total volume fraction of C-S-H LD (including the gel porosity f_{Gel} and volume fraction of solid C-S-H LD f_{LD}^{Sol} from Tennis and Jennings model), f_{HD} is the volume fraction of C-S-H HD, f_{NC} is the volume fraction of non-conductive phases (anhydrates and hydrates other than C-S-H LD). When we assumed that the electrical conductivity of C-S-H HD is $\sigma_{C-S-H} = 0$, we obtain:

$$\sigma_s = \frac{2 f_{LD} \sigma_{PS} \sigma_{CP}^{SC} (f_{LD}^{Sol} - 2 f_{Gel})}{(f_{HD} + f_{NC})(f_{LD}^{Sol} - 2 f_{Gel})\sigma_{PS} - 4 f_{LD} f_s \sigma_{CP}^{SC}} \tag{10}$$

Note that this solution depends on the effective conductivity of the paste σ_{CP}^{SC}, which indicates that the interactions among the phases in the composite play a role in the effective conductivity of the solids. Similar reasoning can be applied to get the MT estimates of σ_s. We have tested such MT estimates assuming either the pore solution or the solids is the matrix and, in both cases, we obtained (nonphysical) negative conductivities of the solids. This result suggests that SC estimates are more adapted to upscale the electrical conductivity of cement pastes. MCM computations (with N_{MC}=10000) were performed to get the SC estimate of σ_s for three w/c (0.3, 0.4, 0.5) and various degree of hydration ($\alpha \in [0, 1]$). We used Eq. 9 (instead of Eq. 10) so that we could account for a σ_{C-S-H} different from 0 (we adopted σ_{C-S-H} of 0, 0.01 and 0.1). When all these scenarios are considered, the resulting mean of σ_s^{MCM} is 0.0246 S/m and a standard deviation of 0.0384 S/m. As expected the standard deviation of the conductivity of the solids is much lower than that associated with the pore solution. Since the standard deviation is on the order of the mean value, a log-normal model of the distribution of σ_s^{MCM} could be used to avoid negative

conductivities. The mean of the conductivity of the solids obtained with MCM is on the order of the values reported in the literature. Coverdale et al. [60], based on numerical investigations, report the value $\sigma_s = 0.01$ S/m. Ma et al. [58], using inverse analysis on cement pastes obtained the empirical expression $\sigma_s^{Emp.}/\sigma_{PS} = 0.00357\left(1 - \frac{1}{1+(2\alpha)^{5.85}}\right)$. Using the typical values of σ_{PS} presented in Fig. 1 (from 1 to 20 S/m), $\sigma_s^{Emp.}$ would range from 0 to 0.07 S/m, which falls in the range of variability of σ_s^{MCM}.

Our bottom-up estimates of σ_s^{MCM} and $\sigma_{PS}(t)$ (from the master curve presented in Fig. 1), and the respective variabilities, can be now used as input in MCM computations associated with Powers model.

Figure 5 shows our estimates compared to the experimental data from Christensen et al. [6]. These authors report the effective electrical conductivity of a cement paste with $w/c = 0.4$ (Fig. 5 (c)) and the capillary porosity of cement pastes with w/c of 0.35 and 0.5 (Fig. 5 (b)). Here, we first estimate the evolution of the degree of hydration for the pastes with w/c of 0.35 and 0.5 from the corresponding results of capillary porosity using Powers model (Appendix B.1). Then, we interpolate the results for a cement paste with w/c =0.4, as shown in Fig. 5 (a), and compute the capillary porosity of this cement paste using Powers model. The effective electrical conductivity of cement paste with $w/c =$ 0.4 (Fig. 5 (c)) is computed according to the SC and MT estimates. Note that, for a two-phase composite, HS upper and lower bounds are identical to the MT estimates using the pore solution as a matrix and using the solid as the matrix, respectively. SC estimate yields result in a better agreement with experimental data than MT estimates. The mean value of conductivity of solids of σ_s^{MCM} is 0.0246 S/m yields estimates in reasonable agreement with the experimental data. Additionally, using a least-squares procedure on the experimental data, we compute the effective conductivity of the solids σ_s^{Fit}=0.027 S/m, which is remarkably closer to σ_s^{MCM}. Furthermore, in order to obtain information regarding the bounds on σ_s, least-squares minimization was also performed for the HS upper and lower bounds: we obtained a σ_s of 0 and 0.13 S/m, respectively.

In contrast with the conductivity of the pore solution, which is reported to

increase with time due to the augmentation of the concentration of mobile ions; the conductivity of the cement paste is expected to decrease with time due to cement hydration processes, which cause a reduction in the capillary porosity. These tendencies are well captured by the SC estimate. The MT estimates using the pore solution as a matrix yield reasonable results for the very early age when the liquid phase functions effectively as a matrix. Accordingly, the MT estimates using the solid phase as a matrix yield reasonable results for late ages, when the solid phase percolates and effectively functions as a matrix. Since no matrix needs to be defined in SC estimations, the corresponding results perform better in capturing the transition from a liquid to a solid matrix during cement hydration.

In this context, the formation factor $F(t)$ can be written using the effective conductivity of the material $\sigma(t)$ and the (time-dependent) conductivity of the pore solution $\sigma_{PS}(t)$: $F(t) = \sigma/\sigma_{PS}(t)$. For a two-phase micro- and macro-isotropic heterogeneous material, the Self-Consistent formation factor F^{SC} is given by:

$$F^{SC}(t) = \frac{1}{4\sigma_{PS}} \left(S'_{SC} + \sqrt{(S'_{SC})^2 + 8\sigma_{PS}\sigma_s} \right) \tag{11}$$

where $S'_{SC} = (3\phi_{cap}(\sigma_{PS} - \sigma_s) - \sigma_{PS} + 2\sigma_s)$, and the time dependencies of the capillary porosity $\phi_{cap}(t)$ and of the electrical conductivity of the pore solution are omitted for conciseness.

In the Fig. 5 (c), the experimental formation factor provided by Christensen et al. [6] for a cement paste with w/c =0.5 is compared with the SC estimates. Again homogenization results provide a good estimation of the early-age development of the effective electrical conductivity of cement paste.

We assess the sensibility of the standard deviation of the effective electrical conductivity of the cement pastes with respect to the variability of the pore solution and solids conductivities in Fig. 6. Figure 6 (b) shows the standard deviation of the effective electrical conductivity of the cement paste as a function of (i) the standard deviation of the conductivity of the pore solution s_{PS} for a

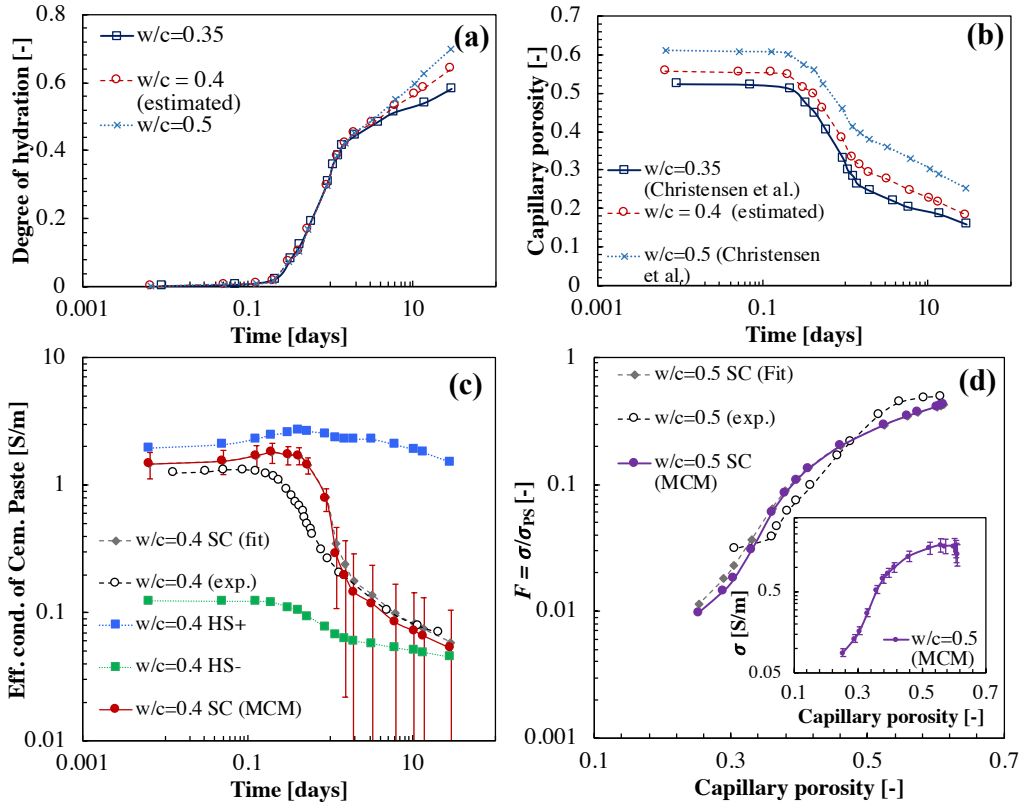

Figure 5: (a) Degree of hydration as a function of the w/c estimated from the capillary porosity in (b) using Powers model. (b) Capillary porosity from Christensen et al. [6] for w/c of 0.35 and 0.5; the capillary porosity for $w/c = 0.4$ was estimated using the corresponding degree of hydration in (a) and Powers model. (c) Effective electrical conductivity of the cement paste with $w/c = 0.4$ as provided by Christensen et al. [6] experiments and homogenization results. SC estimates obtained with MCM (using as input a log-normally distributions for the conductivities of the solids and pore solutions with σ_s=0.0246 S/m and a standard deviations of 0.0384 S/m, and a standard deviation of the pore solution conductivity of 1 S/m) and from least square fitting of the experimental data are shown; HS upper and lower bounds are identical to the MT estimates using the pore solution as a matrix and using the solid as the matrix, respectively. The results of conductivity of the pore solution using the master curve presented in Fig. 1 are used in the homogenization. (d) Formation factor $F = \sigma(t)/\sigma_{PS}(t)$ of a cement paste with $w/c = 0.5$ as a function of the capillary porosity: comparison between experimental [6] and model data ($F^{SC}(t)$). The inset shows the effective electrical conductivity of the cement paste with $w/c = 0.5$ and the associated standard deviation as computed with MCM.

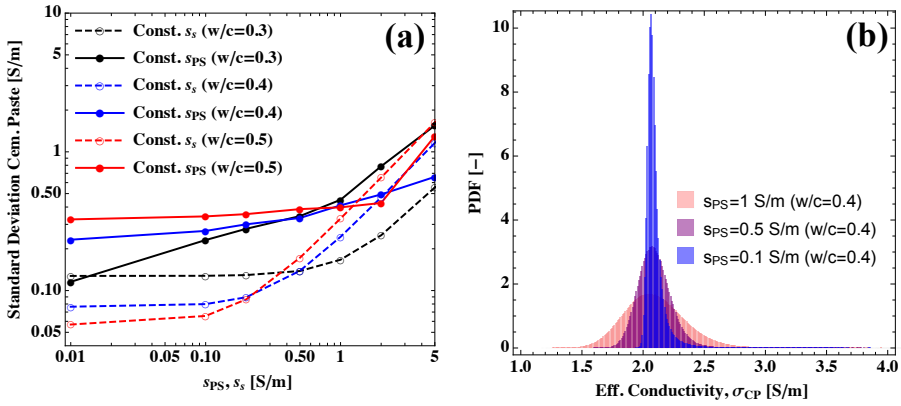

Figure 6: (a) Standard deviation of the effective electrical conductivity of the cement paste as a function of (i) the standard deviation of the conductivity of the pore solution s_{PS} (with s_s=0.0346 S/m), kept constant), and (ii) the standard deviation of the conductivity of the solids s_s (with s_{PS} =1 S/m, kept constant) for cement pastes at 1 day and with w/c ratio of 0.3, 0.4 and 0.5. In all cases the electrical conductivity of the phases are assumed to be log-normally distributed and N_{MC}=5×10^6. (a) Probability Distribution Function (PDF) of the effective electrical conductivity of the cement paste according to the standard deviation of the conductivity of the pore solution s_{PS}, assumed to be log-normally distributed, and a constant standard deviation of the conductivity of the solid phase. Cement paste at 1 day and with w/c =0.4.

constant s_s=0.0384 S/m); and (ii) the standard deviation of the conductivity of the solids s_s for a constant s_{PS} =1 S/m. The results are shown for cement pastes at 1 day with a w/c ratio of 0.3, 0.4 and 0.5. The standard deviation of the cement paste grows faster with the standard deviations of the pore solution than that with the standard deviations of the solids. In Fig. 6 (a), we compare the distributions of the effective conductivity of the cement paste with w/c of 0.4 at 1 day according to three values of s_{PS} and a constant standard deviation of the electrical conductivity of the solid phase (s_s=0.0384 S/m). The distributions of the effective conductivity keep the log-normal character of the conductivities of the constituent phases, being broader as s_{PS} increases.

Accounting for the non-spherical shapes of solid phases in cement-based materials have been considered as a relevant aspect by some authors upscaling the

mechanical properties of cement-based materials [30, 61, 62]. The effects of inclusion shape are expected to be more significant as the contrast of properties increases [9]. It must be noted however that the main contributor to the electrical conductivity of cement-based materials is the pore solution and the pore in such materials are generally modeled as spheres in the framework of micromechanics [30, 61, 62]. Accounting for non-spherical solid phase can affect the estimations of the effective properties of the solids but the expected variations must lies within 0 to σ_{C-S-H} =0.0246 S/m (the maximum conductivity found in the porous solid phase, here C-S-H). In this context, we believe that introducing information on the shape of the solid phase will not contribute to increasing significantly the precision of homogenization estimations. Furthermore, input on at least the aspect ratio distribution (and probably time-dependency) of each phase present would be necessary for a homogenization modeling approach accounting for inclusion shapes. The quantification of hydrates particle shapes is challenging. Theoretical considerations suggest that in the case of C-S-H the particle aspect ratio is time-dependent [51] and larger clusters of C-S-H grains tends to be more elongated [63]. On the other hand, experimental evidence suggests spherical isotropic, fibrils and foils morphologies of C-S-H [64].

3.3. Upscaling the effective electrical properties and variability up to the concrete scale

The effective conductivity of the cement paste, mortar and concrete are presented in Fig. 7 according to various w/c. We adopt a volume fraction of 40% of sand at the mortar scale and 40% of coarse aggregate at the concrete scale. As expected, the conductivity at a given scale and time increases with the w/c. Since the total volume of pores decreases at larger scales, the difference between the effective electrical conductivity of the materials with various w/c decreases the larger are the scales. From the discussion on the transition from a complex fluid to a solid from the last section (see Fig. 5), one may try to correlated the time in which the time derivatives of the conductivity $d\sigma/dt$ conductivity begins to be negative to the setting time. Again, as expected, our

results indicates a setting time that increases with the w/c regardless of the scale considered.

The electrical resistivity $\rho = 1/\sigma$ at the three scales are also shown in Fig. 7. As expected, the resistivity at a given scale and time increases with the decrease of the w/c. The results at the concrete scale are in the same order as the experimental results reported in the literature (e.g. [65, 6, 66]. The non-monotonous aspect of conductivity curves (with a maximum occurring within the first days) has also been observed experimentally [66, 67]. From the functional analysis of SC estimate (Eq. 4), it can be shown (see Appendix D) that a maximum appears at the first hours and the exact time scales decreases with the ratio of the characteristic times associated with pore solution conductivity increase and capillary porosity decrease. If the evolution of capillary porosity and the age-dependency of pore solution conductivity have a similar characteristic time, a maximum in the effective conductivity occurs approximately in the range of 0.1 to 0.5 days. This maximum is therefore not expected to be experimentally probed in most of the cases in which the pastes are tested after setting.

The PDF of the effective electrical conductivity and resistivity of the cement paste, mortar and concrete for various w/c at 1 day are shown in Fig. 8. The log-normal nature of the distribution is also observed in the effective properties. Note that once the distribution of the electrical conductivity (resp. resistivity) is known, the distribution of the resistivity (resp. conductivity) can be computed using the *inverse distribution*. Let X be a random variable with strictly positive support, the PDF f_Y of the random variable $Y = 1/X$ can be computed from the PDF f_X by (e.g. [68]): $f_Y(y) = \frac{1}{y^2} f_X\left(\frac{1}{y}\right)$. Fig. 9 shows that the use of inverse distributions yields results in agreement with MCM estimates. Therefore, information on the statistical variability of one of these properties can be easily used to get the variability of the reciprocal property.

Figure 10 shows the time dependence of the standard deviation of the electrical conductivity and resistivity at the cement paste, mortar and concrete scales for various w/c. Since we consider that the standard deviation of the pore solution conductivity is much larger than the standard deviation of the solids, a

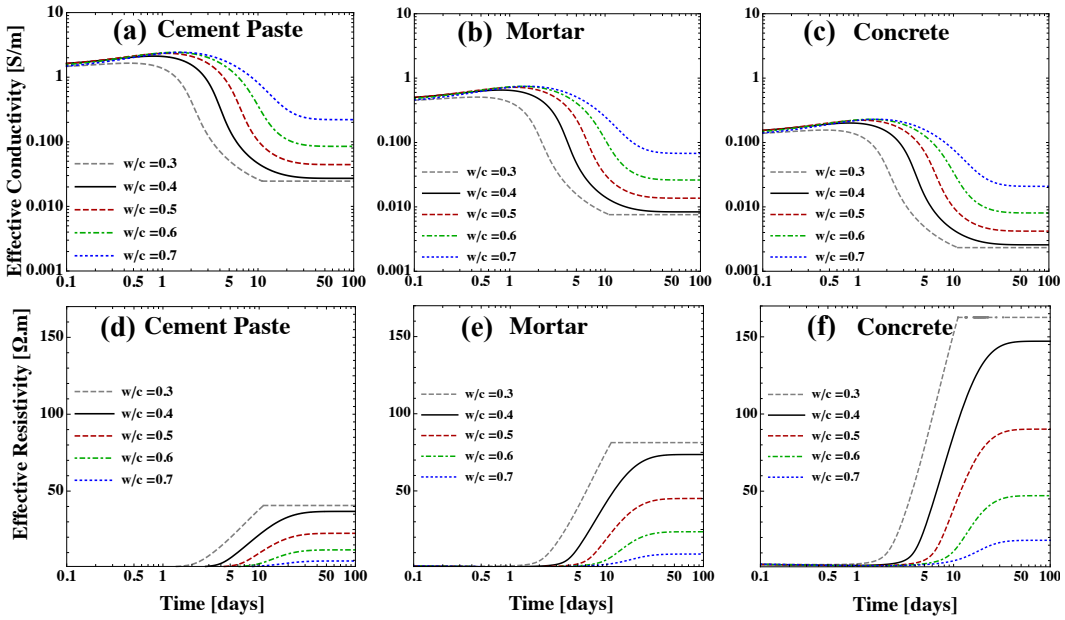

Figure 7: Effective electrical conductivity of (a) cement paste, (b) mortar and (c) concrete scale as a function of the w/c. Effective resistivity of (d) cement paste, (e) mortar and (f) concrete scale as a function of the w/c. We adopt s_{PS} =1 S/m and s_s =0.0384 S/m. The volume fractions of sand at the mortar scale and of coarse aggregate at the concrete scale are 40%.

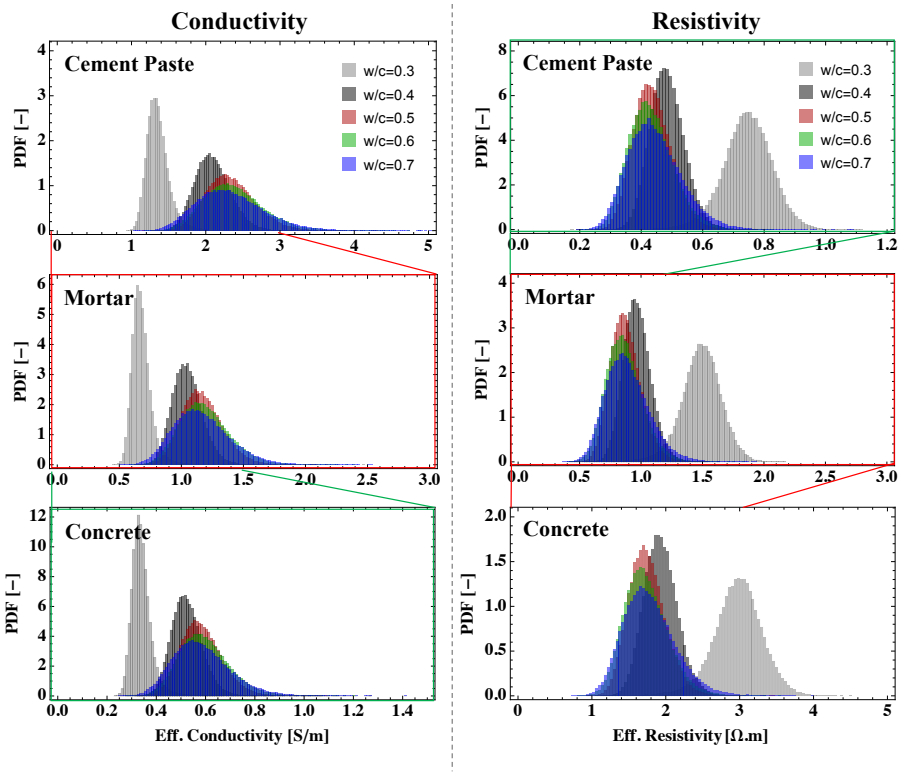

Figure 8: (a) Probability Distribution Function (PDF) of the effective electrical conductivity (at left) and resistivity (at right) at the cement paste, mortar and concrete scales for various w/c at 1 day.

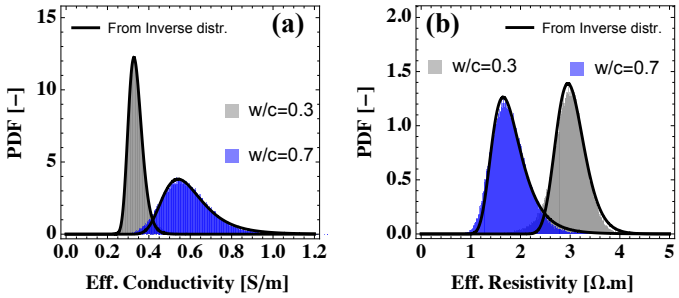

Figure 9: Comparison between the PDF of the effective conductivity at the concrete scale directly computed with MCM and the PDF obtained from the inverse distribution using the results of (a) the resistivity and (b) the conductivity for w/c of 0.3 and 0.7 at 1 day.

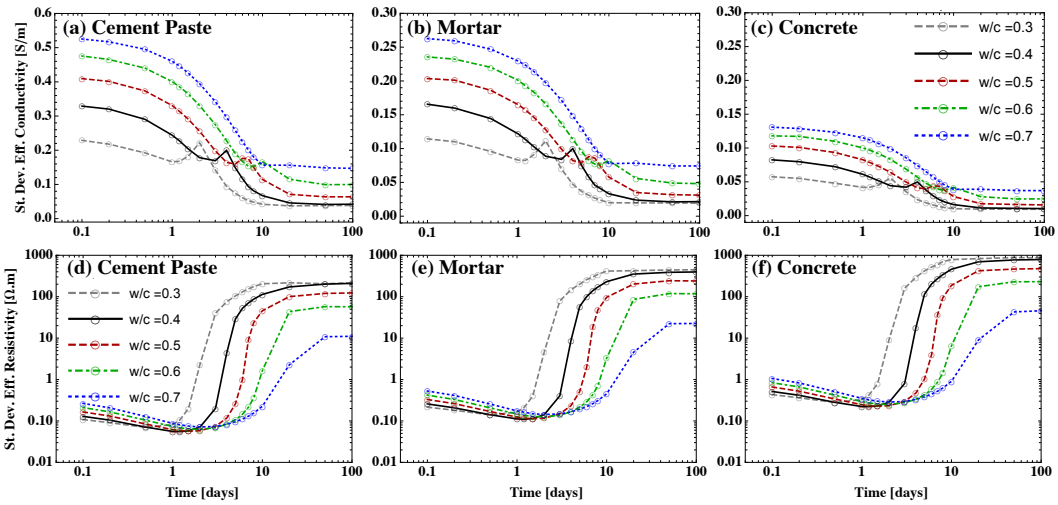

Figure 10: Evolution of the standard deviation of the electrical conductivity (at top) and resistivity (bottom) at the cement paste, mortar and concrete scales for various w/c.

decrease in the effective standard deviations of both conductivity and resistivity with time is observed due to the decrease of the porosity for a given w/c. This effect is more pronounced for lower w/c ratios. The larger the scale, the smaller the variability of the conductivity. This result is expected since most of the variability considered here is associated with the pore phase, whose volume fraction decreases relatively at larger scales. Inverse tendencies are observed in the effective resistivities that increase with time (for a given w/c).

4. Conclusions

In this article, we propose a multiscale modeling approach of the electrical conductivity (and resistivity) of cement-based materials accounting for the variability and age-dependency of the conductivity of the pore solutions. The results obtained in this study are a contribution to a better understanding of the physical origins of cement-based materials properties as well as the cross-relations between transport and electrical properties. These results can be used to reduce the empirism of the interpretation of electrical properties (conductiv-

ity or resistivity) measurements in concrete, especially in applications related to durability and service life prediction of cement-based materials.

Our main conclusions are as follows:

- *Monte Carlo micromechanics (MCM) enables the quantification of the variability and uncertainty across scales.* The variability of the pore solution conductivity is the main ingredient in controlling the variability of the electrical conductivity and resistivity of cement-based materials. Using the inverse distribution, the probability distribution of the resistivity can be linked to the variability of the conductivity. The standard deviation of both resistivity and conductivity decreases with time, and this effect is more pronounced for lower w/c.

- *Self-consistent scheme provides a good estimate of the effective electrical conductivity of cement-pastes capturing the transition from a liquid to a solid matrix during cement hydration.* Using SC estimate in an inverse analysis, we obtained an effective conductivity of the solid σ_s^{MCM} of 0.0246 S/m and a standard deviation of 0.0384 S/m (for a log-normal distribution). This value is larger than the value previously reported in the literature [60] but still two to three orders of magnitude below the conductivities of the pore solution, which means that the solid will effectively function as an electrical insulator. The SC estimate utilized in this work assumes a random microstructure composed of equiaxed heterogeneities and, therefore, does not take into account specific features of the microstructure such as complex inclusion shape, orientation, and distribution. The agreement of our results with experimental data suggests that these specific features are not significant (or, at least, not the main contributors) to the effective electrical properties of cement-based materials.

Perspectives of this study include the consideration of the saturation degree-dependency, thermal activation of ion dynamics and conductivity of pore solutions in cement-based materials.

Acknowledgement

O. Cascudo and H. Carasek would like to thank the company Furnas Centrais Elétricas, from Brazil, for its support in experimental programs concerning the study of electrical resistivity in concretes.

Appendix A. Convergence of MCM and comparison with analytical results

Figure 11 (a) shows the histograms of the effective conductivity of a two-phase isotropic composite mimicking a cement paste obtained using MCM according to various N_{MC}. The matrix corresponds to the solid phase (with a conductivity of 0.1 S/m and a standard deviation of 0.01 S/m) and the inclusions correspond to the pore phase with a conductivity of 10 S/m and standard deviation of 1 S/m according. Both normal or log-normal distributions are considered. The mean and standard deviation of the effective conductivity converge to the analytical value (in which no variability of properties phases is accounted for) for N_{MC} exceeding approximately 10^4, as can be seen in Fig. 11 (b) and (c). This observation is valid for effective conductivities obtained from both normal or log-normal distributions of constituents' properties. Similar results are observed in computations when the solid is taken as the inclusions. To better capture the (a smooth) PDF of the effective conductivities we adopt a N_{MC} of 10^5.

The mean and the variance of a sum S of two independent random variables (denoted by the subscripts $_0$ an $_1$) are given, respectively, by $\mu_S = \mu_0 + \mu_1$ and $s_S^2 = s_0^2 + s_1^2$. Using this property, we can easily compute the effective conductivity of a two-phase composite using a mixture rule (i.e a weighted sum of the properties with respect to the volume fraction of the phases). We compare MCM estimations with analytical results regarding a mixture rule in Fig. 12 for a two-phase isotropic composite (phase 0 has a conductivity of 0.1 S/m and a standard deviation of 0.5 S/m, phase 1 has a conductivity of 10 S/m and standard deviation of 1 S/m) with the properties of the constituents being

Table 1: List of Notations

c_i	molar concentration of ion i
D_i	self-diffusion coefficient of species of type i
D	diffusion coefficient
D_h	homogeneous self-diffusion coefficient
e_{ITZ}	thickness of ITZ
$f(X)$	continuous probability density function on random variable X
$f^{Schulz}(X)$	Schulz distribution of variable X
F	formation factor [-]
F^{SC}	Self-Consistent estimate of the formation factor
$\mathcal{F}$	Faraday constant
f_{Agg}	volume fraction of the aggregates at mortar or concrete scales
f_r	volume fraction of phase r
k	permeability
k_B	Boltzmann constant
l_c	length scale associated with the pores size
m	parameter controlling the variance of Schulz distribution
N_{MC}	number of Monte Carlo trials in MCM
$\vec{P_I}$	ionic polarization
q_i	particle charge
R_{agg}	radius of aggregate
R_g	gas constant
$\vec{r_i}$	position vector of particle i
r_T and s_T	coefficients of thermo-activation of the resistivity and conductivity, respectively
S_{SC}	$= ((3f_1 - 1)\sigma_1 + (2 - 3f_1)\sigma_2)$, term in Eq. 5
s_{LN}	standard deviations of Log-Normal distribution
s_{PS}	standard deviations of electrical conductivity fo the pore solution
s_s	standard deviations of electrical conductivity of the solids
s_X	standard deviation of $f(X)$
t	time
T	temperature
T_1	NMR relaxation time
V	volume
V_{ITZ} and V_{Matrix}	volume of ITZ and volume of the matrix
X and Y	random variable and its reciprocal ($Y = 1/X$)
w/c	water-to-cement mass ratio
z_i	charge number of particle i
α	degree of hydration
ϕ_{cap} and ϕ^0_{cap}	capillary porosity and capillary porosity at t=0
ρ_c ρ_w	mass volume of cement and water
μ_{LN}	mean of Log-Normal distribution
μ_X	mean of $f(X)$
ρ	electrical resistivity
σ	electrical conductivity
σ_{Agg}	electrical conductivity of the aggregates
$\sigma_s^{Emp.}$	empirical conductivity of solids from ref. [58]
$\overline{\sigma_i^{GSC}}$	effective conductivity of a matrix/composite-sphere inclusion material
σ_+^{HS} and σ_-^{HS}	upper and lower Hashin-Shtrikman bounds of the conductivity
σ^{MT}	Mori-Tanaka (or Maxwell-Garnett) estimation of the effective conductivity
σ_{PS}	electrical conductivity of the pore solution
σ_s	electrical conductivity of the solids at cement paste level
σ^{SC}	Self-Consistent (or Bruggeman) estimation of the effective conductivity

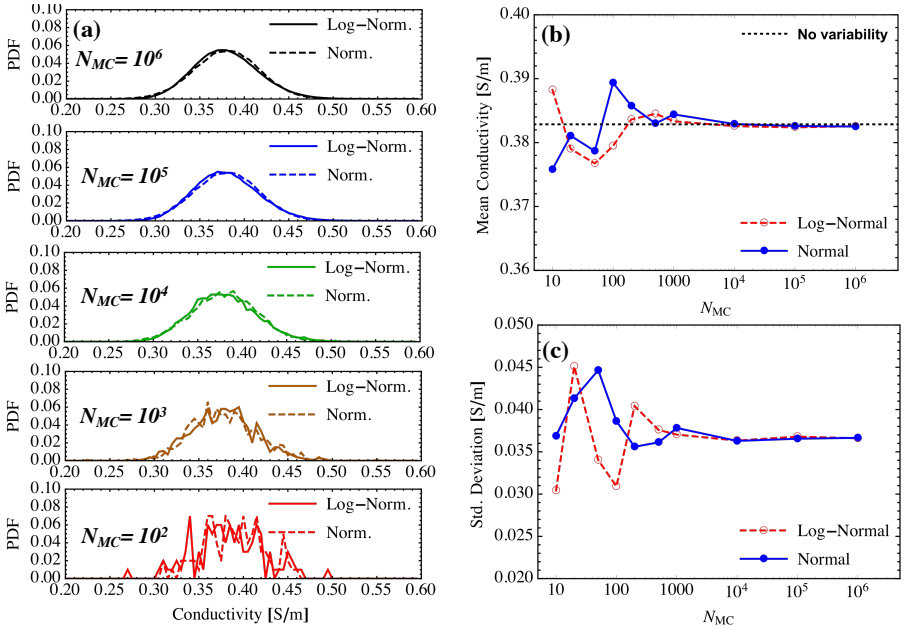

Figure 11: (a) Histograms of effective conductivity obtained using MCM according to various N_{MC}. We consider the MT estimations of a two-phase isotropic composite mimicking a cement paste: matrix with a conductivity of 0.1 S/m and a standard deviation of 0.01 S/m, inclusions with a conductivity of 10 S/m and standard deviation of 1 S/m according to either normal or log-normal distributions. The volume fraction of the inclusions is 0.5. Convergence of the (b) mean and (c) standard deviation of the effective conductivity as a function of the Monte Carlo sample size N_{MC} according to either normal or log-normal distributions of the constituent phases.

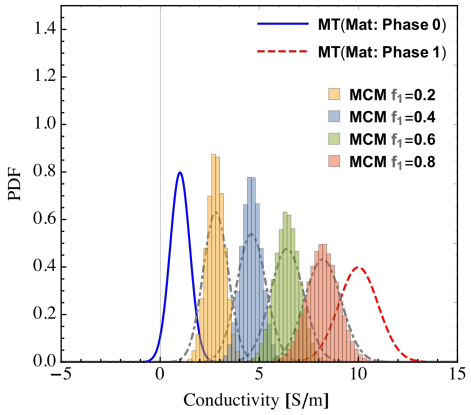

Figure 12: PDF of the effective conductivity obtained from a mixture rule: MCM estimations (N_{MC}=10^5) compared with analytical results (dashed gray curves) for various volume fractions. We consider a two-phase isotropic composite: phase 0 has a conductivity of 0.1 S/m and standard deviation of 0.5 S/m, phase 1 has a conductivity of 10 S/m and standard deviation of 1 S/m. Properties of both are normally distributed. The volume fraction of each phase is 0.5.

normally distributed. The volume fraction of each phase is 0.5. A reasonable agreement is observed between analytical and Monte Carlo results. Note that Monte Carlo sampled moments are generally related to their (exact) ensemble counterparts (even though it is known that they are not expected to coincide (e.g. [69, 70]).

Appendix B. Simplified hydration models

B.1 Powers model

With Powers model (when there is no filler), the volume fractions of the clinker, capillary porosity (or "water"), hydrates and chemical shrinkage (or "air") are provided, respectively [43, 71], as a function of the degree of hydration α by:

$$f_{Clinker} = \frac{1-\alpha}{1+w/c\frac{\rho Clinker}{\rho Water}} = \frac{20(1-\alpha)}{20+63w/c} \geq 0 \tag{12}$$

$$f_{Water} = \frac{(\rho_{Clinker}/\rho_{Water})(w/c - 0.42\alpha)}{1 + w/c\frac{\rho_{Clinker}}{\rho_{Water}}} = \frac{63(w/c - 0.42\alpha)}{20 + 63w/c} \geq 0 \tag{13}$$

$$f_{Hydrates} = \frac{1.42\alpha(\rho_{Clinker}/\rho_{Hydrates})}{1 + w/c\frac{\rho_{Clinker}}{\rho_{Water}}} = \frac{43.15\alpha}{20 + 63w/c} \tag{14}$$

$$f_{Air} = 1 - f_{Clinker} - f_{Water} - f_{Hydrates} = \frac{3.31\alpha}{20 + 63w/c} \tag{15}$$

where $\rho_{Clinker}$=3.15 g/cm^3 is mass volume of clinker, ρ_{Water}=1 g/cm^3 is mass volume of water, and $\rho_{Hydrates}$=2.073 g/cm^3 is mass volume of hydrates [71].

B.2 Tennis and Jennings model

Tennis and Jennings [44] model is based on the stoichiometric equations:

$$2C_3S + 10.6H \rightarrow C_{3.4} - S_2 - H_8 + 2.6CH \tag{16}$$

$$2C_2S + 8.6H \rightarrow C_{3.4} - S_2 - H_8 + 0.6CH \tag{17}$$

$$C_3A + 3C\bar{S}H_2 + 26H \rightarrow C_6A\bar{S}_3H_{32} \tag{18}$$

$$2C_3A + C_6A\bar{S}_3H_{32} + 4H \rightarrow 3C_4A\bar{S}H_{12} \tag{19}$$

$$C_3A + CH + 12H \rightarrow C_4AH_{13} \tag{20}$$

$$C_4AF + 2CH + 10H \rightarrow 2C_3(A, F)H_6 \tag{21}$$

With these relations and the molar volumes of the phases, one can readily compute the volume fractions of the phases as a function of the degree of hydration (or time with a kinetic model is provided). No phases bearing carbonates were originally considered and was assumed that the only aluminum bearing phases

are ettringite ($C_6A\bar{S}_3H_{32}$ or AFt), monosulfoaluminate ($3C_4A\bar{S}H_{12}$ or AFm), hydrogarnet ($2C_3(A,F)H_6$) and C_4AH_{13}. Ettringite is assumed to be completely converted into monosulfoaluminate if water and C_3A are available with the progress of hydration processes. This model allows distinguishing between gel pores, low-density (LD) and high-density (HD) C-S-H. The volume of HD and LD C-S-H is given, respectively, by:

$$V_{HD} = \frac{M_t - (M_r M_t)}{\rho_{HD}};\ V_{LD} = \frac{M_r M_t}{\rho_{LD}} \tag{22}$$

and the volume of gel pore is:

$$V_{Gel\ Pores} = V_{LD} - \frac{M_r M_t}{\rho_{HD}} \tag{23}$$

with ρ_{HD} and ρ_{LD} being the mass volume of HD and LD C-S-H, respectively; M_t is the total mass of C-S-H computed from the stoichiometric relations above; and, $M_r = 3.017(w/c)\alpha - 1.347\alpha + 0.538$ is the LD mass ratio with respect to the M_t.

Figure 13 shows the comparison between the repartitions of the volume fraction of phases obtained with Tennis and Jennings (top) and for Powers' (bottom) models as a function of the degree of hydration for three w/c ratios. The average clinker composition based on Fig. 2(a) was used as input in Tennis and Jennings model.

The evolution of density of C-S-H can be estimated with a combinations of Eqs. 22 and23 :

$$\rho_{C-S-Hgel} = \frac{M_r(\rho_{HD} - \rho_{LD}) + rho_{HD}\rho_{LD}}{2M_r(\rho_{HD} - \rho LD) + \rho_L D} \tag{24}$$

with the values of ρ_{HD} and ρLD proposed by Tennis and Jennings, we observe that $\rho_{C-S-Hgel}$ increases with α but only for $w/c < 0.45$. In this work, no specific steps are introduced to take into account the densification processes of C-S-H but, as shown by Eq. 24, Tennis and Jennings model implies a densification of C-S-H at least approximately for $w/c < 0.45$.

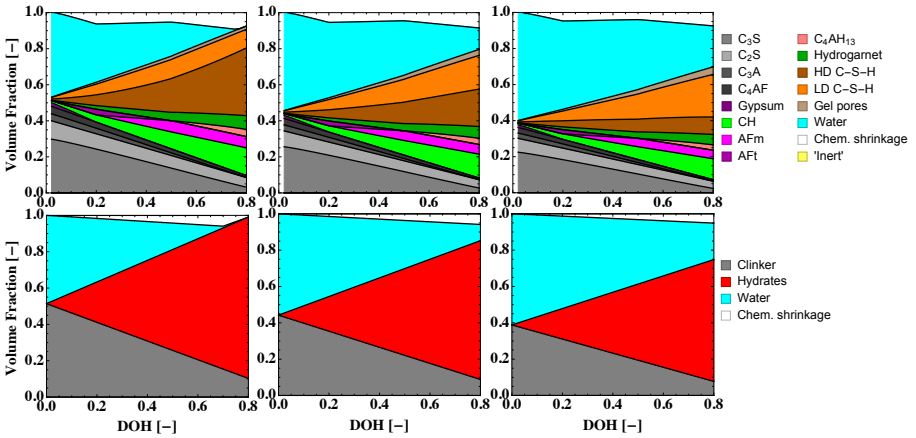

Figure 13: Comparison between the repartitions of the volume fraction of phases obtained with Tennis and Jennings (top) and for Powers' (bottom) models as a function of the degree of hydration for three w/c ratios.

Appendix C. Influence of the ITZ in the effective electrical conductivity

C.1 Accounting for ITZ as an interphase with constant thickness

The presence of ITZ is recognized to play a major role in the strength, diffusive properties and thermal conductivities of cement-based materials [61, 62, 32, 72]. Generalized Self-Consistent (GSC) scheme has been widely deployed to model ITZ [26, 35, 36, 37, 38]. This approach relies, however, in the definition of coatings with a fixed volume fraction with respect to the core irrespective of the core diameter. This aspect is inconsistent with the assumption of an ITZ with a single thickness for all sand aggregate particle sizes.

To overcome this problem, we propose here to use the concept of composite inclusion, associated with the GSC scheme, to fix the thickness of ITZ for all particle sizes in the system. The thickness of ITZ is denoted e_{ITZ}. For a particle with radius R_{Agg}, the effective conductivity of the composite sphere constituted

of a aggregate core embedded in a ITZ coating can be obtained applying Eq. 6:

$$\sigma_{ITZ}^{C}(R_{Agg}) = \sigma_{ITZ} + \frac{3 f_{Agg} \sigma_{ITZ} (\sigma_{Agg} - \sigma_{ITZ})}{(2\sigma_{ITZ} + \sigma_{Agg}) \left(1 - f_{Agg} \frac{(\sigma_{Agg} - \sigma_{ITZ})}{(2\sigma_{ITZ} + \sigma_{Agg})}\right)} \tag{25}$$

where σ_{ITZ} and σ_{Agg} are the conductivity of the ITZ and aggregate particle, respectively; and the term $f_{Agg} = \frac{R_{Agg}^3}{(e_{ITZ}+R_{Agg})^3}$ corresponds to the volume fraction of the aggregate particle in the composite inclusion. A conceptually similar approach, in which a constant ITZ was accounted for according to the Particle Size Distribution (PSD) of the aggregates, was developed by Garboczi and Berryman [73] using the differential scheme. In their application, however, the authors restrict the values of ITZ thickness to few microns, which is below the value experimentally determined by Scrivener et al. [74]. Berryman and

For a system with a polydisperse distribution of aggregates $f_{Agg}(R_{Agg})$, the effective conductivity can be computed using the homogenization schemes presented in the last section by discretizing $f_{Agg}(R_{Agg})$ in i bins and considering each bin as a phase. The volume of interpenetrating ITZ can be computed from the particle size distribution of the aggregates (fine or coarse) using Lu and Torquato results [75], as discussed by Garboczi and Bentz [76].

C.2 Application to the electrical conductivity of mortars

To assess the influence of ITZ, we study various aggregates particle size distributions that can be found in typical mortar and concrete mix design. We adopt the Schulz distribution:

$$f^{Schulz}(X) = \frac{1}{\Gamma(m+1)} \left(\frac{m+1}{\langle X \rangle}\right)^{m+1} X^m exp\left[\frac{-(m+1)X}{\langle X \rangle}\right] \tag{26}$$

where m is a parameter controlling the variance (the variance of the Schulz distribution decreases with m, with $m \to \infty$ the distribution tends to the monodisperse case) and Γ is the gamma function (which is related to the generalization of the factorial function). The nth moment of Schulz distribution is given by $\langle X^n \rangle = \frac{(m+n)!}{m!} \frac{1}{(m+1)^n} \langle X \rangle^n$.

Figures 14(a) and (c) show the passing volume fraction of aggregates according to a three average radius $\langle R_{Agg} \rangle$ (a) and three variances (c) of aggregates particle sizes (controlled through the parameter m of normalized Schulz distribution). For each aggregate size distribution, the corresponding volume fractions of the ITZ (in terms of volume fraction of the matrix: V_{ITZ}/V_{Matrix}) are shown in Figs. 14(b) or (d) as a function of ITZ thickness (in μm). The change of one order of magnitude in the average radius $\langle R_{Agg} \rangle$ impacts more significantly the volume fractions of the ITZ than the change of one order of magnitude in variance parameter m.

The effective electrical conductivities of the composite spheres according to various ITZ thickness e_{ITZ} as a function of the radius of the aggregate are shown in Fig. 15.

Figure 16 shows the effective electrical conductivity of the mortar according to the presence of the ITZ. Accounting for the ITZ becomes significant for aggregate size distributions with an average radius inferior to 1 mm and for the thickness of the ITZ larger than 5 μm. Experimental evidence shows an ITZ thickness in the range 15-20 μm [77]. Therefore, multiscale approaches should ideally take into account the ITZ. However, the attempts to account for ITZ in multiscale modeling must take into account the challenges related to the delimitation of this interfacial zone as well as its composition. The determination of ITZ thickness is not trivial since this interphase exhibits a porosity gradient [74, 37, 38] which make it difficult to place frontier between the ITZ and the bulk cement paste. The gradative variation of porosity may be accompanied by variations in hydrates content. For example, ITZ is reported to present higher Portlandite contents than the bulk paste [74]. In addition, the extension of ITZ can be affected by a factor such as the curing age [78]. Another source of uncertainty related to ITZ is the supplementary porosity contained in this interphase [74, 72]. Curing and water-to-binder ratio are reported to impact ITZ porosity [78]. Considering these uncertainties related to ITZ, in the absence of information on the ITZ features, neglecting the ITZ seems a reasonable choice for the sake of simplicity.

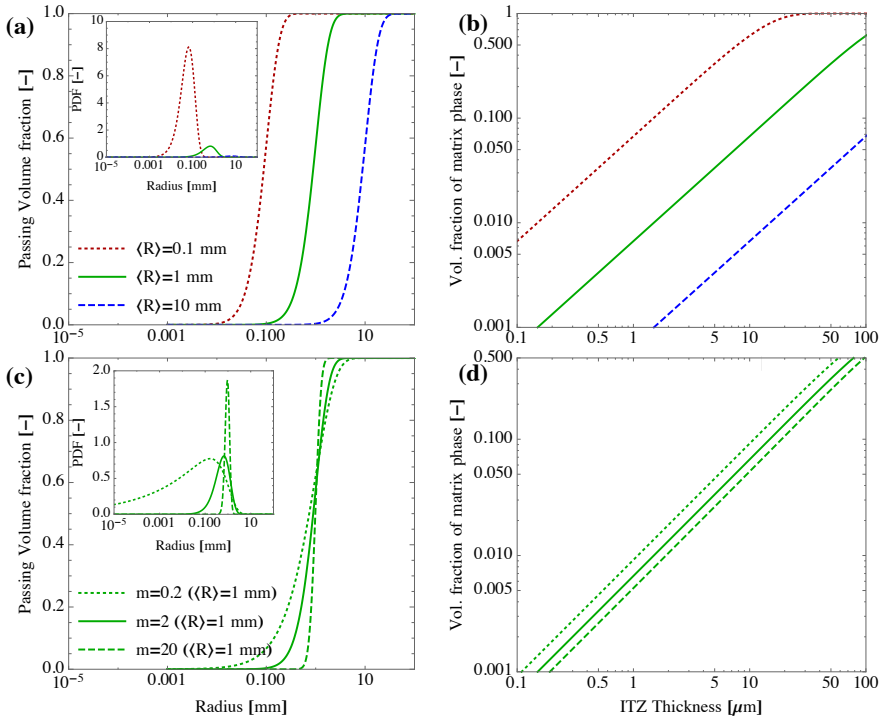

Figure 14: (a) Passing volume fraction of aggregates with three average radius $\langle R \rangle$ for constant variance ($m = 1$). The inset shows the differential size distribution. (b) Volume of ITZ in terms of volume fraction of the matrix (V_{ITZ}/V_{Matrix}) for three different average radius $\langle R_{Agg} \rangle$. (c) Passing volume fraction of aggregates for a constant $\langle R \rangle$ (=1 mm): effect of the variance of aggregates particle sizes (controlled through the parameter m of normalized Schulz distribution). (d) Volume of ITZ in terms of volume fraction of the matrix (V_{ITZ}/V_{Matrix}) according to the parameter m.

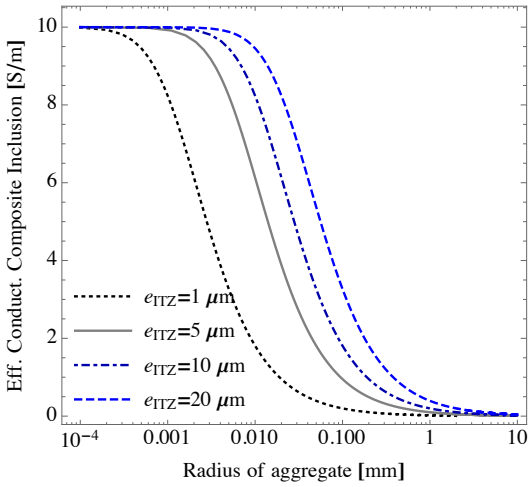

Figure 15: Effective electrical conductivity of the composite spheres with a constant ITZ thickness e_{ITZ} according to the radius of the aggregate.

Finally, it must be notes that the introduction of ITZ

Appendix D. Maximum in the effective electrical conductivity using SC scheme

The SC estimate in Eq. 4 is analyzed to understand the origin of the maximum observed in Fig. 7 at the very early-ages. In Figure 17(a), we compute the effective electrical conductivity of a paste σ_{SC} obtained using as input a conductivity of solids $\sigma_s = 0.01$ S/m and of pore solution $\sigma_{PS}(t) = (10(1 - Exp[-t/\tau_{PS}])$ S/m. The evolution of the capillary porosity is described by $\phi = (0.5Exp[-t/\tau_{CapPor}])$. The kinetics of pore solution composition variation is quantified via the characteristic time τ_{PS}. The kinetics of the capillary porosity evolution is described by the characteristic time τ_{CapPor}. We observe that the maximum appears in SC according to the ratio τ_{PS}/τ_{CapPor}. The age in which the maximum occurs decreases with this ratio, as shown in Fig 17 (b), being limited to ages below 1 day. The analysis of the master curve in Eq. 8 (with a characteristic time of approximately 1 day) and typical evolution of cap-

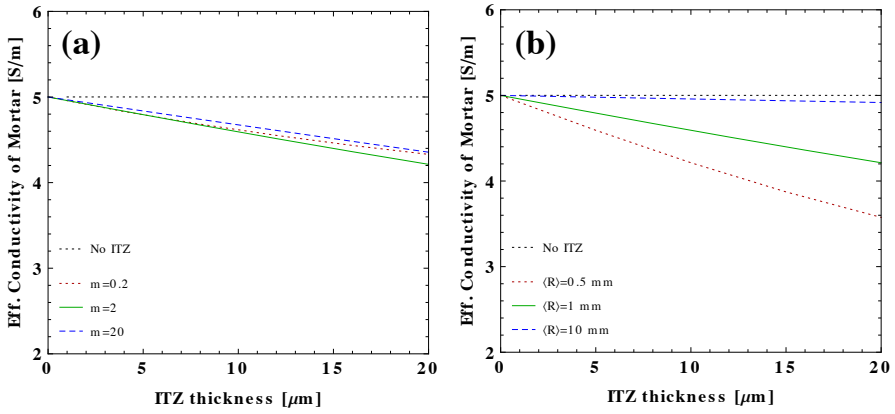

Figure 16: Effective electrical conductivity of the mortar plotted as a function of the ITZ thickness for the aggregate distributions (a) with constant variance ($m = 1$) and three average radius $\langle R_{Agg} \rangle$, (b) for constant average radius ($\langle R_{Agg} \rangle$=1 mm) and three variances (controlled through m parameter).

illary porosity in cement-based materials (with characteristic times on the order of days), shows that the ratio τ_{PS}/τ_{CapPor} is on the order of 1 or below. Thus, for most of the relevant applications in cement-based materials, the maximum is expected to manifest in ages inferior to 1 day.

References

[1] K. R. Gowers, S. G. Millard, Measurement of Concrete Resistivity for Assessment of Corrosion Severity of Steel Using Wenner Technique, ACI Materials Journal 96 (5).

[2] R. Polder, C. Andrade, B. Elsener, Ø. Vennesland, J. Gulikers, R. Weidert, M. Raupach, Test methods for on site measurement of resistivity of concrete, Materials and Structures 33 (10) (2000) 603–611.

[3] X. Wei, Z. Li, Study on hydration of Portland cement with fly ash using electrical measurement, Materials and Structures 38 (3) (2005) 411–417.

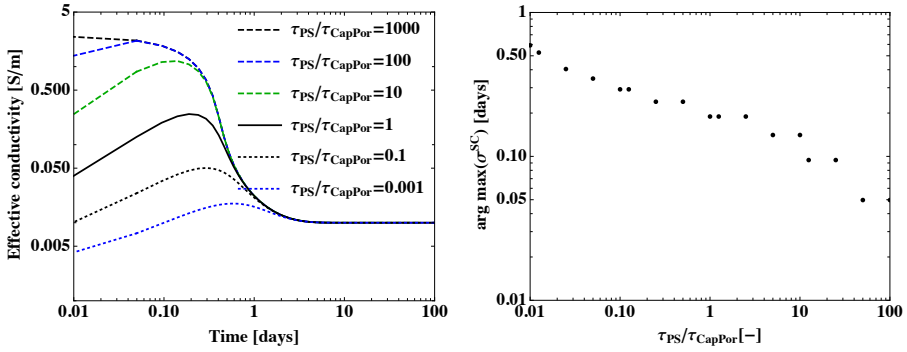

Figure 17: (a) Effective electrical conductivity of a paste σ_{SC} obtained using as input σ_s = 0.01 S/m and pore solution with conductivity $\sigma_{PS}(t) = (10(1 - Exp[-t/\tau_{PS}])$ S/m. The evolution of the capillary porosity is described by $(0.5Exp[-t/\tau_{CapPor}])$. (b) Scaling of the time in which σ_{SC} reaches a maximum with the ratio of characteristic times τ_{PS}/τ_{CapPor}.

[4] S. Tang, X. Cai, Z. He, W. Zhou, H. Shao, Z. Li, T. Wu, E. Chen, The review of early hydration of cement-based materials by electrical methods, Construction and Building Materials 146 (2017) 15–29.

[5] E. J. Garboczi, Permeability, diffusivity, and microstructural parameters: A critical review, Cement and Concrete Research 20 (4) (1990) 591–601.

[6] B. J. Christensen, T. Coverdale, R. A. Olson, S. J. Ford, E. J. Garboczi, H. M. Jennings, T. O. Mason, Impedance Spectroscopy of Hydrating Cement-Based Materials: Measurement, Interpretation, and Application, Journal of the American Ceramic Society 77 (11) (1994) 2789–2804.

[7] M. Avellaneda, S. Torquato, Rigorous link between fluid permeability, electrical conductivity, and relaxation times for transport in porous media, Physics of Fluids A: Fluid Dynamics 3 (11) (1991) 2529–2540.

[8] M. Tsui-Chang, A. N. Amirkhanian, P. Suraneni, R. P. Spragg, A. T. Coyle, W. J. Weiss, Activation Energy of Conduction for Use in Temperature Corrections on Electrical Measurements of Concrete, Advances in Civil Engineering Materials 8 (1) (2019) 158–170.

[9] S. Torquato, Random Heterogeneous Materials: Microstructure and Macroscopic Properties, Springer Science & Business Media, 2002.

[10] L. V. Gibiansky, S. Torquato, Link between the conductivity and elastic moduli of composite materials, Physical Review Letters 71 (18) (1993) 2927–2930.

[11] K. Hornbostel, C. K. Larsen, M. R. Geiker, Relationship between concrete resistivity and corrosion rate – A literature review, Cement and Concrete Composites 39 (2013) 60–72.

[12] B. Lothenbach, F. Winnefeld, Thermodynamic modelling of the hydration of Portland cement, Cement and Concrete Research 36 (2) (2006) 209–226.

[13] A. Vollpracht, B. Lothenbach, R. Snellings, J. Haufe, The pore solution of blended cements: a review, Materials and Structures 49 (8) (2016) 3341–3367.

[14] T. Honorio, F. Benboudjema, T. Bore, M. Ferhat, E. Vourc'h, The pore solution of cement-based materials: structure and dynamics of water and ions from molecular simulations, Physical Chemistry Chemical Physics 21 (2019) 11111–11121.

[15] E. J. Garboczi, D. P. Bentz, Modelling of the microstructure and transport properties of concrete, Construction and Building Materials 10 (5) (1996) 293–300.

[16] Y. Zuo, J. Zi, X. Wei, Hydration of cement with retarder characterized via electrical resistivity measurements and computer simulation, Construction and Building Materials 53 (2014) 411–418.

[17] K. Van Breugel, Simulation of hydration and formation of structure in hardening cement-based materials, Ph.D. thesis, Delft (1991).

[18] D. P. Bentz, CEMHYD3d: A Three-Dimensional Cement Hydration and Microstructure Development Modeling Package, Tech. Rep. Version 3.0.

NISTIR 7232., National Institute of Standards and Technology (NIST), Interagency Report, Technology Administration, U.S. Department of Commerce, NISTIR 7232 (Jun. 2005).

[19] S. Bishnoi, K. L. Scrivener, ic: A new platform for modelling the hydration of cements, Cement and Concrete Research 39 (4) (2009) 266–274.

[20] E. Berodier, K. Scrivener, Evolution of pore structure in blended systems, Cement and Concrete Research 73 (2015) 25–35.

[21] T. Mura, Micromechanics of defects in solids, 2nd Edition, Mechanics of elastic and inelastic solids. Editors: S. Nemat-Nasser and G. AE. Oravas, Martinus Nijhoff Publishers, 1987.

[22] J. Ma, I. Temizer, P. Wriggers, Random homogenization analysis in linear elasticity based on analytical bounds and estimates, International Journal of Solids and Structures 48 (2) (2011) 280–291.

[23] J. Ma, J. Zhang, L. Li, P. Wriggers, S. Sahraee, Random homogenization analysis for heterogeneous materials with full randomness and correlation in microstructure based on finite element method and Monte-carlo method, Computational Mechanics 54 (6) (2014) 1395–1414.

[24] J. Lataste, T. De Larrard, F. Benboudjema, J. Semenadisse, Study of electrical resistivity: variability assessment on two concretes: protocol study in laboratory and assessment on site, European Journal of Environmental and Civil Engineering 16 (3-4) (2012) 298–310.

[25] G. W. Milton, The Theory of Composites, Cambridge University Press, Cambridge, 2002.

[26] A. Ulrik Nilsen, P. J. M. Monteiro, Concrete: A three phase material, Cement and Concrete Research 23 (1) (1993) 147–151.

[27] O. Bernard, F.-J. Ulm, E. Lemarchand, A multiscale micromechanics-hydration model for the early-age elastic properties of cement-based materials, Cement and Concrete Research 33 (9) (2003) 1293–1309.

[28] C. J. Haecker, E. J. Garboczi, J. W. Bullard, R. B. Bohn, Z. Sun, S. P. Shah, T. Voigt, Modeling the linear elastic properties of Portland cement paste, Cement and Concrete Research 35 (10) (2005) 1948–1960.

[29] M. Wyrzykowski, J. Sanahuja, L. Charpin, M. Königsberger, C. Hellmich, B. Pichler, L. Valentini, T. Honório, V. Smilauer, K. Hajkova, G. Ye, P. Gao, C. Dunant, A. Hilaire, S. Bishnoi, M. Azenha, Numerical benchmark campaign of COST Action TU1404 – microstructural modelling, RILEM Technical Letters 2 (2017) 99–107.

[30] J. Sanahuja, L. Dormieux, G. Chanvillard, Modelling elasticity of a hydrating cement paste, Cement and Concrete Research 37 (10) (2007) 1427–1439.

[31] S. Ghabezloo, Micromechanics analysis of thermal expansion and thermal pressurization of a hardened cement paste, Cement and Concrete Research 41 (5) (2011) 520–532.

[32] T. Honorio, B. Bary, F. Benboudjema, Thermal properties of cement-based materials: Multiscale estimations at early-age, Cement and Concrete Composites 87 (2018) 205–219.

[33] B. Bary, S. Béjaoui, Assessment of diffusive and mechanical properties of hardened cement pastes using a multi-coated sphere assemblage model, Cement and Concrete Research 36 (2) (2006) 245–258.

[34] Z. Hashin, S. Shtrikman, A variational approach to the theory of the effective magnetic permeability of multiphase materials, Journal of Applied Physics 33 (10) (1962) 3125–3131.

[35] Z. Hashin, P. J. M. Monteiro, An inverse method to determine the elastic properties of the interphase between the aggregate and the cement paste, Cement and Concrete Research 32 (8) (2002) 1291–1300.

[36] T. Honorio, B. Bary, J. Sanahuja, F. Benboudjema, Effective properties of n-coated composite spheres assemblage in an ageing linear viscoelastic framework, International Journal of Solids and Structures 124 (2017) 1–13.

[37] J. C. Nadeau, Water–cement ratio gradients in mortars and corresponding effective elastic properties, Cement and Concrete Research 32 (3) (2002) 481–490.

[38] J. C. Nadeau, A multiscale model for effective moduli of concrete incorporating ITZ water–cement ratio gradients, aggregate size distributions, and entrapped voids, Cement and Concrete Research 33 (1) (2003) 103–113.

[39] Z. Hashin, Thin interphase/imperfect interface in conduction, Journal of Applied Physics 89 (4) (2001) 2261–2267.

[40] V. Sansalone, S. Naili, C. Desceliers, A stochastic homogenization approach to estimate bone elastic properties, Comptes Rendus Mécanique 342 (5) (2014) 326–333. doi:10.1016/j.crme.2013.12.007.
URL http://www.sciencedirect.com/science/article/pii/S1631072114000746

[41] T. Honorio, H. Carasek, O. Cascudo, May self-diffusion of ions computed from molecular dynamics explain the electrical conductivity of pore solutions in cement-based materials?, under review.

[42] T. Honorio, T. Bore, F. Benboudjema, E. Vourc'h, M. Ferhat, Dielectric properties of the pore solution in cement-based materials, Journal of Molecular Liquids (2020) 112548doi:10.1016/j.molliq.2020.112548.

[43] T. C. Powers, Physical properties of cement paste, in: Proceedings of the Fourth International Symposium on Chemistry of Cement, Washington, 1960, pp. 577–613.

[44] P. D. Tennis, H. M. Jennings, A model for two types of calcium silicate hydrate in the microstructure of Portland cement pastes, Cement and Concrete Research 30 (2000) 855–863.

[45] T. Honorio, Correlation between the composition variability of Ordinary Portland Cement and the elastic properties of pastes: a Monte Carlo Micromechanics study, Pre-print.

[46] H. F. W. Taylor, Cement chemistry, 2nd Edition, T. Telford, London, 1997.

[47] T. Honorio, T. Lemaire, D. D. Tommaso, S. Naili, Molecular modelling of the heat capacity and anisotropic thermal expansion of nanoporous hydroxyapatite, Materialia (2019) 100251.

[48] T. Honorio, B. Bary, F. Benboudjema, Multiscale estimation of ageing viscoelastic properties of cement-based materials: A combined analytical and numerical approach to estimate the behaviour at early age, Cement and Concrete Research 85 (2016) 137–155.

[49] A. C. A. Muller, K. L. Scrivener, A. M. Gajewicz, P. J. McDonald, Densification of C–S–H Measured by 1H NMR Relaxometry, The Journal of Physical Chemistry C 117 (1) (2012) 403–412. doi:10.1021/jp3102964. URL http://dx.doi.org/10.1021/jp3102964

[50] M. Königsberger, C. Hellmich, B. Pichler, Densification of C-S-H is mainly driven by available precipitation space, as quantified through an analytical cement hydration model based on NMR data, Cement and Concrete Research 88 (2016) 170–183. doi:10.1016/j.cemconres.2016.04.006. URL http://www.sciencedirect.com/science/article/pii/S0008884616303374

[51] M. Königsberger, B. Pichler, C. Hellmich, Multiscale poro-elasticity of densifying calcium-silicate hydrates in cement paste: An experimentally validated continuum micromechanics approach, International Journal of Engineering Science 147 (2020) 103196. doi:10.1016/j.ijengsci.2019.103196. URL http://www.sciencedirect.com/science/article/pii/S0020722519322700

[52] J. O. Bockris, A. K. N. Reddy, Modern Electrochemistry 2B: Electrodics in Chemistry, Engineering, Biology and Environmental Science, Springer Science & Business Media, 2000.

[53] K. R. Harris, M. Kanakubo, Self-diffusion, velocity cross-correlation, distinct diffusion and resistance coefficients of the ionic liquid [BMIM][Tf $_2$ N] at high pressure, Physical Chemistry Chemical Physics 17 (37) (2015) 23977–23993.

[54] X. Lu, Application of the Nernst-Einstein equation to concrete, Cement and Concrete Research 27 (2) (1997) 293–302.

[55] K. A. Snyder, J. Marchand, Effect of speciation on the apparent diffusion coefficient in nonreactive porous systems, Cement and Concrete Research 31 (12) (2001) 1837–1845.

[56] E. J. Garboczi, D. P. Bentz, Computer simulation of the diffusivity of cement-based materials, Journal of Materials Science 27 (8) (1992) 2083–2092.

[57] R. T. Coverdale, B. J. Christensen, H. M. Jennings, T. O. Mason, D. P. Bentz, E. J. Garboczi, Interpretation of impedance spectroscopy of cement paste via computer modelling, Journal of Materials Science 30 (3) (1995) 712–719.

[58] H. Ma, D. Hou, J. Liu, Z. Li, Estimate the relative electrical conductivity of C–S–H gel from experimental results, Construction and Building Materials 71 (2014) 392–396.

[59] T. Honorio, L. Brochard, B. Bary, Statistical variability of mechanical fields in thermo-poro-elasticity: Multiscale analytical estimations applied to cement-based materials at early-age, Cement and Concrete Research 110 (2018) 24–41.

[60] R. T. Coverdale, E. J. Garboczi, H. M. Jennings, B. J. Christensen, T. O. Mason, Computer Simulation of Impedance Spectroscopy in Two Dimensions: Application to Cement Paste, Journal of the American Ceramic Society 76 (6) (1993) 1513–1520.

[61] M. Königsberger, B. Pichler, C. Hellmich, Micromechanics of ITZ-Aggregate Interaction in Concrete Part I: Stress Concentration, Journal of the American Ceramic Society 97 (2) (2014) 535–542.

[62] M. Königsberger, M. Hlobil, B. Delsaute, S. Staquet, C. Hellmich, B. Pichler, Hydrate failure in ITZ governs concrete strength: A micro-to-macro validated engineering mechanics model, Cement and Concrete Research 103 (2018) 77–94.

[63] K. Ioannidou, M. Kanduč, L. Li, D. Frenkel, J. Dobnikar, E. Del Gado, The crucial effect of early-stage gelation on the mechanical properties of cement hydrates, Nature Communications 7 (2016) 12106. doi:10.1038/ncomms12106.
URL http://www.nature.com/ncomms/2016/160715/ncomms12106/full/ncomms12106.html#affil-auth

[64] Z. Zhang, G. W. Scherer, A. Bauer, Morphology of cementitious material during early hydration, Cement and Concrete Research 107 (2018) 85–100. doi:10.1016/j.cemconres.2018.02.004.
URL http://www.sciencedirect.com/science/article/pii/S0008884617310992

[65] K.-Y. Liao, P.-K. Chang, Y.-N. Peng, C.-C. Yang, A study on characteristics of interfacial transition zone in concrete, Cement and Concrete Research 34 (6) (2004) 977–989.

[66] X. Hu, C. Shi, X. Liu, J. Zhang, G. de Schutter, A review on microstructural characterization of cement-based materials by AC impedance spectroscopy, Cement and Concrete Composites 100 (2019) 1–14.

[67] W. J. McCarter, T. M. Chrisp, G. Starrs, A. Adamson, P. A. M. Basheer, S. V. Nanukuttan, S. Srinivasan, C. Green, Characterization of physiochemical processes and hydration kinetics in concretes containing supplementary cementitious materials using electrical property measurements, Cement and Concrete Research 50 (2013) 26–33.

[68] M. C. Jones, On reciprocal symmetry, Journal of Statistical Planning and Inference 138 (10) (2008) 3039–3043.

[69] A. Mood, F. Graybill, D. Boes, Introduction to the theory of statistics, 3rd Edition, McGraw-Hill, 1974.

[70] F. Ballio, A. Guadagnini, Convergence assessment of numerical Monte Carlo simulations in groundwater hydrology: TECHNICAL NOTE, Water Resources Research 40 (4).

[71] B. Pichler, C. Hellmich, Upscaling quasi-brittle strength of cement paste and mortar: A multi-scale engineering mechanics model, Cement and Concrete Research 41 (5) (2011) 467–476.

[72] E. Stora, B. Bary, Q.-C. He, On Estimating the Effective Diffusive Properties of Hardened Cement Pastes, Transport in Porous Media 73 (3) (2008) 279–295.

[73] E. J. Garboczi, J. G. Berryman, New Effective Medium Theory for the Diffusivity or Conductivity of a Multi-Scale Concrete Microstructure Model | NIST, Concrete Science and Engineering 2.

[74] K. L. Scrivener, A. K. Crumbie, P. Laugesen, The Interfacial Transition Zone (ITZ) Between Cement Paste and Aggregate in Concrete, Interface Science 12 (4) (2004) 411–421.

[75] B. Lu, S. Torquato, Nearest-surface distribution functions for polydispersed particle systems, Physical Review A 45 (8) (1992) 5530–5544.

[76] E. J. Garboczi, D. P. Bentz, Analytical formulas for interfacial transition zone properties, Advanced Cement Based Materials 6 (3–4) (1997) 99–108.

[77] K. L. Scrivener, T. Füllmann, E. Gallucci, G. Walenta, E. Bermejo, Quantitative study of Portland cement hydration by X-ray diffraction/Rietveld analysis and independent methods, Cement and Concrete Research 34 (9) (2004) 1541–1547.

[78] Y. Gao, G. De Schutter, G. Ye, Z. Tan, K. Wu, The ITZ microstructure, thickness and porosity in blended cementitious composite: Effects of curing age, water to binder ratio and aggregate content, Composites Part B: Engineering 60 (2014) 1–13.